

# Inertial waves near corotation in 3D hydrodynamical disks

Henrik N. Latter<sup>\*</sup> and Steven A. Balbus<sup>†</sup>

*Laboratoire de Radioastronomie, École Normale Supérieure, 24 rue Lhomond, Paris 75005, France*

20 October 2009

## ABSTRACT

This paper concerns the interaction between non-axisymmetric inertial waves and their corotation resonances in a hydrodynamical disk. Inertial waves are of interest because they can localise in resonant cavities circumscribed by Lindblad radii, and as a consequence exhibit discrete oscillation frequencies that may be observed. It is often hypothesised that these trapped eigenmodes are affiliated with the poorly understood QPO phenomenon. We demonstrate that a large class of non-axisymmetric 3D inertial waves cannot manifest as trapped normal modes. This class includes any inertial wave whose resonant cavity contains a corotation singularity. Instead, these ‘singular’ modes constitute a continuous spectrum and, as an ensemble, are convected with the flow, giving rise to shearing waves. Lastly, we present a simple demonstration of how the corotation singularity stabilizes three-dimensional perturbations in a slender torus.

**Key words:** accretion, accretion disks — hydrodynamics — instabilities — waves

## 1 INTRODUCTION

Inertial waves, also called r-modes (Korycansky and Pringle 1995, Ogilvie 1998) or g-modes (Wagoner 1999, Kato 2001a), are one of a rich assortment of oscillations exhibited by hydrodynamical models of accretion disks. They may be distinguished by a number of interesting properties: first, they comprise motions that are effectively incompressible, and which strongly couple the vertical and horizontal velocities. Second, their oscillation frequencies take values much less than the local epicyclic frequency, which suggests that inertial waves figure prominently in a disk’s response to low frequency forcing (Balbus 2003), such as might issue from an embedded protoplanet. Third, these modes are the only waves that propagate in the vicinity of their corotation resonances, i.e. the radii where their pattern speed is zero. Finally, in principle they may become trapped between their two Lindblad resonances and hence manifest as a discrete suite of standing modes (see, for example, Okazaki et al. 1987, Perez et al. 1997).

Inertial waves have been invoked to explain various astrophysical phenomena, but of special interest is their potential role in the excitation of the quasi-periodic oscillations (QPOs) that are observed in the X-ray spectra of some black-hole disk systems (e.g., Wagoner 1999; Kato 2001a, McClintock and Remillard 2003). The idea is that since the inertial modes appear as trapped standing waves, they (or their resonant interactions) may exhibit oscillation frequencies in accord with the observed frequencies. Mean-

while, a variety of instabilities have been promoted in order to explain the large amplitudes necessary for the detection of these frequencies (Abramowicz and Kluźniak 2001, Kato 2001b, 2003b, Ferreira and Ogilvie 2008, for example).

Though axisymmetric waves (Okazaki et al. 1987) and certain non-axisymmetric waves (Perez et al. 1997) have been demonstrated mathematically to form discrete trapped standing waves, this behaviour has not been established satisfactorily for general three-dimensional modes. In this paper we show, with both WKB techniques and direct methods, that in most cases, three-dimensional inertial waves do not manifest this way. This is because most non-axisymmetric 3D modes possess a corotation singularity within their resonant cavity. While earlier work (Kato 2003a, Li et al. 2003) has shown how the corotation singularity damps incident wave fluxes, it has not been generally appreciated that the corotation singularity also very likely *prohibits* the formation of trapped normal modes themselves. The present paper is concerned with investigating the dynamics of this problem. In addition, we study the continuous spectrum that issues from the corotation singularity, showing its close relationship with inertial shearing waves (Johnson and Gammie 2005, Balbus and Hawley 2006). Lastly, we demonstrate how the wave absorption at corotation impedes unstable three-dimensional modes in a slender torus. In so doing, we deepen our understanding of the complicated and varied linear responses available to accretion disks.

The outline of this paper is as follows. Section 2 presents the governing equations of an incompressible disk in a shearing sheet and summarises the main qualitative features of travelling inertial waves near the corotation point. Section 3 demonstrates the absence of trapped modes around corota-

<sup>\*</sup> E-mail: henrik.latter@lra.ens.fr

<sup>†</sup> E-mail: steven.balbus@lra.ens.fr

tion by solving the boundary value problem. In the following section we provide details of a WKBJ analysis which supplies the same result in a more realistic semi-global model but in the limit of large vertical wavenumber. Section 5 outlines the relationship between shearing waves and the continuous spectrum induced by the corotation singularity, while Section 6 describes instability in a 3D slender torus. Our conclusions are drawn in Section 7.

## 2 PRELIMINARIES

Our treatment is restricted to inertial waves whose resonant cavities contain the corotation singularity. Such a configuration is typical for 3D inertial waves in both Newtonian and (general) relativistic disks, with only a narrow band of non-axisymmetric r-modes in relativistic disks exhibiting a different configuration of resonances (see Perez et al. 1997, Waggoner 1999, Kato 2001a, 2001b). The more common modes were first studied in detail by Kato (2002), who suggested that the corotation point could give rise to a form of the Papaloizou-Pringle instability. Subsequent WKBJ and numerical analyses, however, demonstrated that an incident inertial wave would be strongly absorbed at corotation (Kato 2003a, Li et al. 2003, but see Drury, 1985, for a much earlier discussion). These results convinced researchers that such trapped 3D modes must decay. As a consequence, the emphasis of much ‘diskoseismology’ has moved on to other mechanisms of instability, typically involving a parametric resonance (Abramowicz and Kluźniak 2001, Kato 2003b, Ferreira and Ogilvie 2008). However, a central question remains unaddressed: How is it possible that trapped standing waves (growing or decaying) form at all in the vicinity of a strong wave absorber, such as the corotation singularity?

The WKBJ analysis of Kato (2002, 2003a; hereafter K02 and K03a), assumes the existence of such trapped modes and computes their damping rates. The theory incorporates neither explicit nor implicit dissipation, which allows a growing mode for each decaying mode present, due to time symmetry. But because the problem exhibits a branch cut, this symmetry must be broken in any calculation. At the outset, one must assume either growth or decay of the modes to be studied. Henceforth, care must be taken to assure self-consistency. Both K02 and K03a assumed that their modes grow in their calculation. Their final result, however, was that the modes decay. This was treated, not as an inconsistency to be rectified, but as indication the modes do, in fact, decay. It is the view of the authors that the correct interpretation of the inconsistency is that there exists no trapped modes at all. The only class of modes that could in principle resolve the contradiction are strictly neutral. But such modes are singular, possessing undefined radial derivatives at the critical point.

In Section 4 we revisit the analysis of K02 and K03a and reestablish the above result in some detail. Before doing so, we demonstrate the main ideas using a simple local model, the shearing sheet, and very straightforward techniques. In the shearing sheet limit, the trapped wave problem can be solved analytically, and hence is more readily understood. This limit neglects global phenomena such as curvature terms and edge effects, as well as general rela-

tivity, but it includes all the essential physics: a corotation singularity with two Lindblad resonances on either side.

We begin with the basic equations in the shearing sheet limit, and then give a brief summary of travelling inertial waves. This will help us interpret the results of the following section in which the absence of normal modes is demonstrated.

### 2.1 Governing equations

The shearing sheet (Goldreich and Lynden-Bell 1965) is designed to study local disk behavior. We make the additional assumptions that self-gravity is unimportant, and that the fluid is incompressible. Also, we work in the ‘cylindrical limit’: the equilibrium density is unstratified, independent of both cylindrical radius ( $r$ ) and height ( $z$ ). It can be shown, however, that the vertical stratification plays no role in the qualitative behaviour of our problem. For example, an isothermal model yields analogous results, at greater mathematical cost (see Appendix A).

The governing equations in the shearing sheet read:

$$\partial_t \mathbf{u} + \mathbf{u} \cdot \nabla \mathbf{u} + 2\Omega_0 \mathbf{e}_z \times \mathbf{u} = -\nabla \Phi - \frac{1}{\rho} \nabla p, \quad (1)$$

$$\nabla \cdot \mathbf{u} = 0, \quad (2)$$

where  $\mathbf{u}$  is velocity,  $\Phi$  is the tidal potential,  $p$  is pressure, and  $\rho$  is density (assumed a constant). Additionally,  $\Omega_0 \equiv \Omega(r_0)$  is the local orbital frequency of the disk, where  $r_0$  is the radius at which the shearing sheet is anchored. The  $x$ -coordinate represents radius ( $dx = dr$ ), the  $y$  coordinate the azimuthal direction ( $dy = r d\theta$ ), and the  $z$  coordinate the vertical direction. The sheet undergoes a background linear shear flow

$$\mathbf{u}_0 = -q\Omega_0 x \mathbf{e}_y \quad (3)$$

where  $q = -(d \ln \Omega / d \ln r)_0$ . If the disk is Keplerian,  $q = 3/2$ . Henceforth, the 0 subscript on  $\Omega_0$  will be suppressed.

### 2.2 Linear perturbation equations

The governing equations admit by construction the homogeneous equilibrium  $\mathbf{u} = \mathbf{u}_0$ ,  $\rho = \rho_0$ , and  $p = p_0$ . Let us now introduce a small disturbance so that  $\mathbf{u} = \mathbf{u}_0 + \mathbf{u}'$ , and  $p = p_0 + p'$ . The equations governing the linear evolution of such a perturbation are:

$$\partial_t u'_x - q\Omega x \partial_y u'_x - 2\Omega u'_y = -\partial_x h', \quad (4)$$

$$\partial_t u'_y - q\Omega x \partial_y u'_y + \frac{1}{2}(\kappa^2/\Omega)u'_x = -\partial_y h', \quad (5)$$

$$\partial_t u'_z - q\Omega x \partial_y u'_z = -\partial_z h', \quad (6)$$

with the incompressibility restriction:

$$\partial_x u'_x + \partial_y u'_y + \partial_z u'_z = 0. \quad (7)$$

Note that the perturbed enthalpy  $h' = p'/\rho_0$  takes the place of the perturbed pressure  $p'$ . The epicyclic frequency is defined through  $\kappa^2 = 2(2 - q)\Omega^2$ .

The perturbations are Fourier decomposed in space so that each mode is  $\propto \exp(ik_y y + ik_z z)$ . The adoption of sinusoidal variation in  $z$  is permitted by the cylindrical approximation. After some manipulation we arrive upon the central equation of the linear analysis for a single mode  $(k_y, k_z)$ ,

$$(\partial_t - iq\Omega x k_y)^2 (\partial_x^2 - k_\perp^2) u'_x + \kappa^2 k_z^2 u'_x = 0, \quad (8)$$

where  $k_\perp^2 \equiv k_y^2 + k_z^2$ , and  $u'_x$  now represents a Fourier amplitude. At this point we perform a temporal Fourier transform and assume the equation admits discrete modal solutions, i.e. we take  $u'_x \propto e^{-i\omega t}$ , where  $\omega$  is a (complex) frequency. We set

$$\omega = \omega_r + i\sigma,$$

for  $\omega_r$  and  $\sigma$  real. The sign of  $\sigma$  must be specified now so as to negotiate the branch point that arises from the inviscid dynamics. Without loss of generality we set  $\sigma \geq 0$ , as the inviscid problem supports either neutral modes or growing/decaying pairs (due to the time symmetry). Equation (8) is now

$$\tilde{\omega}^2 \partial_x^2 u'_x + (\kappa^2 k_z^2 - k_\perp^2 \tilde{\omega}^2) u'_x = 0, \quad (9)$$

where

$$\tilde{\omega} = \omega + q\Omega x k_y. \quad (10)$$

### 2.3 Wave-shape equation

In order to achieve a simpler version of our working equation, a shifted dimensionless space variable is adopted,

$$x^* = k_\perp \left( x + \frac{\omega_r}{q\Omega k_y} \right). \quad (11)$$

Hence we anchor the shearing sheet upon the radius in the disk at which the mode is convected by the shear flow. The star is dropped hereafter for notational convenience, in addition to the subscript  $x$  and prime on  $u'_x$ . The central wave-shape equation of the analysis is consequently

$$\partial_x^2 u + \left[ \frac{\beta^2}{(x - ix_c)^2} - 1 \right] u = 0, \quad (12)$$

where

$$x_c = -\frac{\sigma}{q\Omega k_y}. \quad (13)$$

It will be assumed, without loss of generality, that  $k_y > 0$  and so  $x_c < 0$ . The dimensionless parameter  $\beta$  is defined through

$$\beta = \left| \frac{\kappa(k_z/k_y)}{q\Omega} \right|. \quad (14)$$

In fact,  $\beta^2$  is directly analogous to the Richardson number (Booker and Bretherton, 1967, and see Li et al., 2003), and measures the ratio of the stabilizing effects of rotation, embodied in the term  $\kappa^2(k_z^2/k_y^2)$ , against the destabilising effects of shear.

The governing wave-shape equation possesses a singularity at  $x = ix_c$  (the corotation point). However, the solutions are regular for real  $x$  provided that  $x_c \neq 0$ , meaning that the solutions must grow (or decay). Strictly neutral modes (for which  $x_c = 0$ ) are undefined because they have singular derivatives. With  $\sigma > 0$ , and  $x_c < 0$ , the singularity always lies beneath the real axis, which serves as our contour of integration. Thus the branch cut extending to the left of the singularity always lies beneath the integration contour.

The singularity corresponds to the corotation resonance, and arises because the fluid is inviscid; it vanishes when dissipation is added. Note also that the singularity depends on  $k_z \neq 0$  (from Eq.(14)), and is not present for

two-dimensional modes. The two Lindblad resonances occur at

$$x = \pm\beta + ix_c,$$

which are arranged symmetrically around the corotation radius. (This symmetry is broken when curvature effects are included.) The resonant cavity is defined by  $|x| \leq \beta$ . Density waves can propagate outside of this region, but because the fluid is incompressible, the ‘evanescent zones’ extend to positive and negative infinity.

Trapped standing waves must decay far from corotation in the evanescent zones:  $|u| \rightarrow 0$  when  $|x| \rightarrow \infty$ . Equation (12) is then a one-dimensional eigenvalue problem with eigenvalue  $\sigma$ . In fact, Eq. (12) is a form of the Bessel equation and so the general solution can be written in closed form immediately

$$u = a_1 \sqrt{x - ix_c} I_\nu(x - ix_c) + b_1 \sqrt{x - ix_c} I_{-\nu}(x - ix_c) \quad (15)$$

where  $a_1$  and  $b_1$  are constants,  $I_\nu(z)$  is a modified Bessel function of first kind, and the order  $\nu$  is defined through

$$\nu = \frac{1}{2} \sqrt{1 - 4\beta^2}, \quad (16)$$

(see, for example, Abramowitz and Stegun, 1972). This is particularly advantageous as, unlike other work, we need not resort to WKBJ or Frobenius approximations. The former corresponds to the limit of large imaginary order  $\nu$  (i.e.  $\beta \gg 1$ ) and the latter to small argument  $x$ . Two classes of solution can be distinguished. When  $\beta > 1/2$  (corresponding to modes with greater wavevector pitch  $k_z/k_y$ ) the order of the Bessel functions  $\nu$  is imaginary and strongly oscillatory solutions are obtained. When  $\beta \leq 1/2$  the profiles resemble hyperbolic trigonometric functions.

Before we attack the boundary value problem we discuss free travelling waves within the resonant cavity. This will illuminate some of the properties of the standing waves near corotation and help us understand in more physical terms the results of Section 3. Some of this analysis also appears in Booker and Bretherton (1967), Vishniac and Diamond (1989), and Li et al. (2003).

### 2.4 Free inertial waves near corotation

We first discuss the properties of wave-like solutions to (9) far from corotation  $\tilde{\omega} = 0$  by making the familiar WKBJ ansatz,  $u = R(x)e^{i\psi(x)}$ , where  $\psi$  is a phase function that varies rapidly with  $x$  in comparison with  $R$ . We make the identification  $k_x \equiv \partial_x \psi$  and also assume that  $k_y \sim k_z \sim k_x$ . This ansatz is substituted into (9) and we collect terms of order  $k_x^2$ . These assumptions lead to the dispersion relation for inertial waves,

$$\tilde{\omega}^2 = \frac{k_z^2}{k^2} \kappa^2, \quad (17)$$

where  $k^2 = k_x^2 + k_y^2 + k_z^2$  (see also Balbus 2003). The group velocity of these waves with respect to the Doppler-shifted frequency  $\tilde{\omega}$  is given by

$$\mathbf{V} = \nabla_{\mathbf{k}} \tilde{\omega} = \frac{\tilde{\omega}}{k^2} (-k_x, -k_y, (k_x^2 + k_y^2)/k_z), \quad (18)$$

where  $\mathbf{k} = (k_x, k_y, k_z)$ . Clearly,  $\mathbf{k} \cdot \mathbf{V} = 0$  and the group velocity is perpendicular to the phase velocity. Moreover,

the sign of the radial component of the group velocity  $V_x$  depends on both  $\mathbf{k}$  and the sign of  $\tilde{\omega}$ , and consequently the location of the wave relative to the corotation point. Inside corotation ( $\tilde{\omega} < 0$ ), the group velocity points in the *same* radial direction as that of the phase velocity. But, outside corotation ( $\tilde{\omega} > 0$ ), the group velocity points in the *opposite* radial direction to the phase velocity.

Next we treat the fate of the inertial waves as they approach corotation, assuming that the group velocity calculated above does not deviate significantly in this region. Near this radius a Frobenius solution may be employed. From Eq. (15), to leading order the approximation is

$$u = a_1 (x - ix_c)^{1/2+\nu} + b_1 (x - ix_c)^{1/2-\nu}, \quad (19)$$

where  $a_1$ ,  $b_1$  and  $\nu$  are the same quantities introduced earlier. We adopt the WKBJ approximation and thus assume  $\beta$  is large; now  $\nu \approx i\beta$ . Consequently, a local radial wavenumber can be defined for each of the two solution components above. In particular,

$$u = \sqrt{x - ix_c} \left( a_1 e^{i\beta \ln |x - x_c|} + b_1 e^{-i\beta \ln |x - x_c|} \right). \quad (20)$$

The  $(x - x_c)^{i\beta}$  component possesses  $k_x = \beta/x$ , and consequently we identify the  $a_1$  function as a left-going wave (moving from positive to negative  $x$ ). This is because when  $x > 0$  then  $k_x > 0$ , and so, according to Eq. (18), the radial component of the group velocity  $V_x$  is negative. When  $x < 0$ , then  $k_x < 0$ , and  $V_x$  will also be negative. A similar argument establishes that the  $b_1$  function is the wave propagating to the right (moving from negative to positive  $x$ ).

When one of these wave components passes through corotation, it will be strongly absorbed, suffering an amplitude damping proportional to  $e^{-\pi\beta}$ . This is clear from the analytic continuation of the Frobenius solution Eq. (19) through the corotation region, noting that the singularity  $x = ix_c$  lies beneath the real line, and thus beneath the integration contour. For large  $\beta$ , i.e. large wavevector pitch  $k_z/k_y$ , the incident waves barely penetrate the corotation barrier. For general  $\beta$ , when each wave passes through corotation from its proper direction, its amplitude will acquire a factor

$$\exp\left(\frac{1}{2}i\pi + i\pi\nu\right), \quad (21)$$

from (19). For  $\beta \leq 1/2$ , the alteration corresponds to a phase shift of  $\pi(\nu + 1/2)$ . But it nevertheless gives rise to a damping of angular momentum and energy flux through the corotation point (Li et al. 2003).

It is this damping that has led researchers to discount the possibility of instability in this context: the corotation resonance is a powerful barrier against the communication of wave motions, plundering energy from potentially growing modes. We now show that this barrier not only precludes instability, it precludes standing modes entirely.

### 3 ABSENCE OF TRAPPED 3D INERTIAL WAVES IN THE SHEARING SHEET MODEL

In this section we take the exact solution (15) to the governing wave-mode equation (12) and show that it cannot satisfy the two decaying boundary conditions at  $|x| \rightarrow \infty$ .

Physically, the reason for this is that the standing mode consists of a precise balance of two traveling waves (the left and right-going WKBJ waves of the previous section) and the corotation point will heavily damp one component relative to the other. Consequently, the correct balance of components on one side of corotation will never correspond to the correct balance on the other side of corotation.

Mathematically, the result is straightforward. The boundary condition at  $x \rightarrow \infty$  forces  $u$  to be proportional to the Bessel function of second kind  $K_\nu(x - ix_c)$  for all  $x$ , as long as  $x_c \neq 0$ . This function, however, diverges when  $x \rightarrow -\infty$  and so no solution exists.

Even though the mathematics is clear, we develop this problem in some detail because it sheds light on the physics of the mode prohibition. In particular, it shows that the problem issues from the fundamental interaction between a wave and its corotation singularity, and is thus quite general — not an artefact of the shearing sheet model. After all, the shearing sheet also prohibits  $k_z = 0$  modes (for which there is no singularity) because of its simple linear shear (by analogy with Case 1960). Moreover, the lengthier treatment below helps us deal with the nontrivial  $x_c = 0$  case, which sets up a treatment of ‘singular modes’ and the continuous spectrum.

#### 3.1 Boundary conditions

We apply the boundary condition  $|u| \rightarrow 0$  as  $|x| \rightarrow \infty$  upon the general solution to (12),

$$u = a_1 \sqrt{x - ix_c} I_\nu(x - ix_c) + b_1 \sqrt{x - ix_c} I_{-\nu}(x - ix_c). \quad (22)$$

Normally these constraints would lead to two algebraic equations for  $b_1/a_1$  and  $x_c$ . Determining the latter is the ‘eigenvalue problem’, or ‘quantisation condition’. As we shall see, such an equation does not appear in this problem.

Throughout this section, we take  $\beta$  large (WKBJ waves) and so make the approximation  $\nu \approx i\beta$ . Each solution component above can then be regarded as a travelling wave: the  $I_{i\beta}$  component corresponds to  $(x - x_c)^{i\beta}$  and the left-travelling wave, while the  $I_{-i\beta}$  component corresponds to the right-travelling wave. These two must be balanced appropriately in order to form a localised standing wave. Lastly, recall that  $k_y > 0$  and thus  $x_c < 0$ . The sign of  $x_c$  is important in what follows as it determines the asymptotic forms of the Bessel functions far from corotation.

Consider first the limit  $x \rightarrow \infty$ . The asymptotic forms of the two solution components can be derived using

$$I_{i\beta}(X) = \frac{1}{\sqrt{2\pi X}} \left( e^X + ie^{-\pi\beta - X} \right),$$

where  $X = x - ix_c$  (Abramowitz and Stegun 1972). To force the solution  $u$  to decay when  $x$  is large and positive, the coefficient of  $\exp(x)$  must be set to zero, and this gives us the relation

$$b_1/a_1 = -1. \quad (23)$$

This combination means that  $u$  is proportional to  $K_\nu(x - ix_c)$ , the associated Bessel function of second kind (mentioned above).

Consider next the other side of the critical point in the limit  $x \rightarrow -\infty$ . The correct asymptotic form to use in this

region is

$$I_{i\beta}(X) = \frac{e^{-\pi\beta}}{\sqrt{2\pi X}} \left( -e^{-\pi\beta+X} + ie^{-X} \right),$$

because the argument of  $X$  approaches  $-\pi$  from below (Abramowitz and Stegun 1972). In order to satisfy the boundary condition for large negative  $x$ , the coefficient of  $\exp(-x)$  must be zero. But this condition does not lead to a constraint on  $x_c$ . Instead, we obtain

$$b_1/a_1 = e^{-2\pi\beta}, \quad (24)$$

which is incompatible with Eq. (23). For large  $\beta$  the ratio (24) is tiny. This very small ratio compensates for the severe damping that the left-travelling wave  $I_{i\beta}$  suffers in this region (see Eq. (21)).

The requirement for two different linear combinations precludes the existence of a continuous analytic solution. There are no normal modes: when  $\sigma \neq 0$  the solution is not continuous at  $x = 0$ , when  $\sigma = 0$  the solution is continuous, but possesses undefined derivatives at  $x = 0$ , a difficulty that can not be resolved whatever the sign of  $\sigma$ .

Let us attempt to understand this mathematical difficulty in more physical terms. The reason for the two incompatible linear combinations is the heavy damping caused by the singularity near  $x = 0$ : this strong damping prevents the simultaneous satisfaction of the two boundary conditions. The correct combination of waves in the region  $x > 0$  violates the boundary condition in the  $x < 0$  region and vice versa. For example, suppose we take the correct combination of components in  $x > 0$  and analytically continue this solution into the  $x < 0$  region (in so doing passing above the singularity, as always). When our solution passes through the vicinity of corotation, the (right-going)  $I_{-i\beta}$  component will abruptly pick up an ‘amplification’ factor  $e^{\pi\beta}$  (because we are proceeding ‘backward in time’ with respect to this wave), while the  $I_\nu$  component picks up a damping factor  $e^{-\pi\beta}$  (as we are proceeding forward in time). As a consequence, the amplitudes of the two waves will differ by  $e^{-2\pi\beta}$ . But this large difference will upset the balance necessary to satisfy the decaying boundary condition at negative infinity, which requires the two components to be of comparable amplitude (at the very least). Thus as  $x$  becomes large and negative,  $u$  will blow up because it will be dominated by the coefficient of  $e^{-x}$  that issues from  $I_\nu$ . If we take the correct combination of waves in  $x < 0$  and follow them into  $x > 0$  the same problem is encountered.

For small  $\beta$  (less than  $1/2$ ), the order of the Bessel functions  $\nu$  is real and each solution component picks up a phase shift, rather than an amplitude change, when it is followed through corotation (see Eq. (21)). But this phase shift is also sufficient to prohibit the formation of normal modes as before: if we remove the divergent component of the solution when  $x \rightarrow \infty$ , the phase jump across  $x = 0$  means we are unable to remove the divergent component of the solution at  $x \rightarrow -\infty$ .

Though there exist no analytic eigenfunctions, when  $\sigma = 0$  a piecewise solution can be devised which is continuous at  $x = 0$  but whose derivative, as already noted, is undefined at this point:

$$u_s = \Theta(x)u_+(x) + \Theta(-x)u_-(x), \quad (25)$$

where  $\Theta(x)$  is the Heaviside step function and the right and

left functions are

$$u_+ = a_1^* x^{1/2} [I_\nu(x) - I_{-\nu}(x)], \quad (26)$$

$$u_- = b_1^* x^{1/2} [I_\nu(x) + e^{2i\nu} I_{-\nu}(x)], \quad (27)$$

where  $a_1^*$  and  $b_1^*$  are two undetermined constants. In fact, because of translational symmetry, we can define such a neutral singular ‘mode’ at each  $x$ . As an ensemble this set of structures (understood as ‘weak’ or ‘distributional’ solutions) defines a continuous spectrum, because each radius is a singularity for at least one mode. Associated with the non-normal operators which appear regularly in shear flow problems, such ‘solutions’ aid in the evolution of initial data and thus only have physical meaning as kernels in the integral expressions of  $u$  (see for example Schmid and Henningson, 2001). In particular, the continuous spectrum is often responsible for transient growth effects. The initial value problem we address in Appendix C, and in Section 5 where we show the relationship between the continuous spectrum and shearing waves.

In summary, this simple demonstration shows the main problem trapped inertial waves suffer if they are to form around their corotation singularity. The shearing sheet model, though probably inadequate to fully describe inertial waves in real relativistic disks, here suffices to illustrate the principal physical and mathematical issues at play. In short, the absence of normal modes stems from the selective wave damping at the corotation radius. As a consequence, potential standing waves, composed of both right and left-travelling waves can never be calibrated so that they decay in the far field on either side of corotation. (In Appendix A these results are generalised to a slightly incompressible fluid, and in Appendix B the influence of viscosity is considered.)

## 4 ABSENCE OF TRAPPED INERTIAL WAVES IN A SEMI-GLOBAL MODEL

In this section, we present a WKBJ calculation in a more realistic semi-global model of a disk. In the limit of large  $k_z$ , the main result of the previous section is recovered. The analysis is similar to, but somewhat simpler than, the development in K02. Nevertheless, it is still involved and the reader may skip directly to Section 5 without loss of continuity.

Our strategy is to first assume that trapped standing waves grow,  $\sigma > 0$ , then to determine their approximate profiles near the two Lindblad resonances (subsections 4.2.1 and 4.2.2 and 4.3) and near the corotation resonance (subsection 4.2.3), and finally to match these three solutions in the WKBJ regions which border their domains of validity (subsection 4.4). The matching conditions supply an eigenvalue equation (58) for the growth rate  $\sigma$  of the trapped modes. We approximately solve this equation, as in K02, and determine that in fact  $\sigma < 0$ . We conclude, as a consequence, that no such trapped modes can exist.

### 4.1 The wave-mode equation

We begin with an incompressible disk in cylindrical geometry  $(r, \phi, z)$  orbiting with frequency profile  $\Omega(r)$ . If the

isothermal approximation is used, the dynamics remain essentially unaltered (though more mathematically involved). The system admits an equilibrium state characterised by the (constant) density  $\rho_0$  and the flow  $\mathbf{u} = r\Omega \mathbf{e}_\phi$ . A small perturbation taking the form  $\propto \exp(im\phi + ik_z z - i\omega t)$  is governed by the following linearised equations,

$$i\tilde{\omega}u'_r + 2\Omega u'_\phi = \partial_r h', \quad (28)$$

$$i\tilde{\omega}u'_\phi - \kappa^2/(2\Omega) u'_r = i(m/r)h', \quad (29)$$

$$i\tilde{\omega}u'_z = ik_z h', \quad (30)$$

$$0 = u'_r/r + \partial_r u'_r + i(m/r)u'_\phi + ik_z u'_z, \quad (31)$$

where  $h = p'/\rho_0$  and  $\tilde{\omega} = \omega - m\Omega$ . The epicyclic frequency is defined through  $\kappa^2(r) = 2\Omega(r\partial_r\Omega + 2\Omega)$  but, in order to approximately account for general relativistic effects near a black hole,  $\kappa(r)$  may take other forms (see Okazaki et al. 1987, Kato 1990).

This set can be manipulated into a simple second order ODE for  $u'_r$ , which may be significantly simplified (as in K02) by assuming that the mode oscillates rapidly in comparison with the radial variation of the background equilibrium. If

$$\partial_r \ln \kappa, \partial_r \ln \Omega \sim K,$$

where  $K$  is some characteristic wavenumber, then  $K \ll k_z$ . Also we let

$$u'_r/r \ll \partial_r u'_r \sim k_z u'_r, \quad k_z \gg m/r.$$

If we normalize the unit of length so that  $K = 1$ , the wave-shape equation is approximated by

$$\partial_r^2 u'_r + \epsilon^2 f(r, \omega) u'_r = 0 \quad (32)$$

where

$$f(r, \omega) = \frac{\kappa^2 - \tilde{\omega}^2}{\tilde{\omega}^2}, \quad (33)$$

and  $\epsilon = k_z/K$  is a large dimensionless parameter. Equation (32) is analogous to Eq.(9) in Section 2 and Eq. (20) in K02. For notational ease, hereafter we drop the prime and  $r$  subscript on  $u'_r$ .

Equation (32) possesses two turning points  $R_1$  and  $R_2$ , the inner and outer Lindblad resonances, which are defined through

$$\tilde{\omega} = -\kappa, \quad \tilde{\omega} = \kappa$$

respectively. These two radii circumscribe a resonant cavity in which low frequency standing waves may localise. In addition, there exists the corotation singularity  $R_c$  defined through  $\tilde{\omega} = 0$ . As noted by Kato (2001b, 2002), for nonzero  $m$ , this point usually falls between  $R_1$  and  $R_2$ , though there exists a small interval of  $\omega$  for which this is not the case (see Perez et al. 1997). This special circumstance is not investigated here and we assume  $R_{1r} < R_{cr} < R_{2r}$  (where the  $r$  subscript indicates real part). Because the resonant cavity contains the corotation singularity, neutral modes are prohibited. Consequently, if trapped normal modes are to exist, they must occur in growing/decaying pairs.

We set  $\omega = \omega_r + i\sigma$  where  $\omega_r$  and  $\sigma$  are real and  $0 < \sigma \ll \Omega$ . The analysis is hence limited to slow growing modes. As a consequence,  $R_1$ ,  $R_2$  and  $R_c$  gain small imaginary parts.

These can be approximated, to leading order in  $\sigma$ , by

$$R_{1i} = \frac{\sigma}{m\Omega'_1 - \kappa'_1}, \quad (34)$$

$$R_{2i} = \frac{\sigma}{m\Omega'_2 + \kappa'_2}, \quad (35)$$

$$R_{ci} = \frac{\sigma}{m\Omega'_c}, \quad (36)$$

where a prime indicates differentiation with respect to  $r$ , and a subscript of 1, 2, or  $c$  indicates evaluation at  $r = R_{1r}$ ,  $R_{2r}$ , or  $R_{cr}$  respectively. Even if  $\kappa$  is assumed to possess a turning point near  $R_{cr}$  (as it will in the inner part of a general relativistic disk) it is easy to see that  $R_{1i}$ ,  $R_{2i}$ , and  $R_{ci}$  are negative for all  $m$  and that

$$R_{1i} < R_{ci} < R_{2i}.$$

#### 4.1.1 ‘Rossby-wave term’

Before continuing we draw attention to the ‘Rossby-wave term’ that will become important when some of the scaling assumptions are relaxed — namely, if we let  $k_y \sim k_z$ , and suppose there exist localised regions where the orbital frequency varies rapidly. If this were the case, the function  $f$  would pick up the following term,

$$\frac{(m/r) \partial_r (\kappa^2/\Omega)}{2k_z^2 \tilde{\omega}}. \quad (37)$$

This simple pole may give rise to ‘Rossby wave instability’ in two-dimensional ( $k_z = 0$ ) dynamics (Lovelace et al. 1999, Li et al. 2000), though for the large  $k_z$  scalings we employ here Rossby modes do not appear. In particular, near corotation  $\tilde{\omega} = 0$  the Rossby wave term is dominated by the double pole in (33). Having said that, it is conceivable that when  $k_z$  is small and the orbital frequency possesses a localised region of exceptionally strong shear, instability could arise. If so there will exist a critical  $k_z$  above which the double pole dominates the dynamics and consequently eliminates potential Rossby wave instability. We do not attempt calculate this critical vertical wavenumber here, though we do investigate similar behaviour in Section 6 with respect to the Papaloizou-Pringle instability in a slender torus (see also Sternberg et al. 2008). In any case, realistic  $\Omega$  and  $\kappa$  profiles are unlikely to exhibit such strong variation; if Rossby-wave instability is to occur it will probably have to rely on steep density gradients (which we have excluded with the assumption of incompressibility).<sup>1</sup>

## 4.2 Approximate solutions near the Lindblad and corotation resonances

### 4.2.1 Inner Lindblad radius

Near  $r = R_1$  we can let  $f = \alpha_1(r - R_1)$  to leading order, where  $\alpha_1 = \partial_r f$  evaluated at  $r = R_1$ . The wave-mode equation subsequently takes the form of a complex Airy’s equation

$$\partial_r^2 u + \epsilon^2 \alpha_1 (r - R_1) u = 0,$$

<sup>1</sup> We thank the reviewer for bringing this issue to our attention.

with solution

$$u = a_1 \text{Ai}[\beta_1(R_1 - r)] + b_1 \text{Bi}[\beta_1(R_1 - r)], \quad (38)$$

in which  $\text{Ai}[z]$  and  $\text{Bi}[z]$  are the two Airy functions,  $a_1$  and  $b_1$  are two complex constants, and

$$\beta_1 = \epsilon^{2/3} \alpha_1 (-\alpha_1)^{-2/3}. \quad (39)$$

The constant  $\alpha_1$  will possess a small imaginary component whose sign plays an important role in negotiating the Stokes phenomenon we encounter later. For small  $\sigma$  we can approximate the imaginary part of  $\alpha_1$  with the compact expression

$$\text{Im}(\alpha_1) = -\frac{2\sigma}{\kappa_1} \left( \frac{\partial}{\partial r} \ln \left[ \frac{\kappa' - m\Omega'}{\kappa} \right] \right)_1. \quad (40)$$

As earlier, the subscript 1 indicates evaluation at  $r = R_{1r}$ . If the logarithm is expanded it is easy to see that the right hand side is positive. Then we can write

$$\beta_1 = \epsilon^{2/3} \alpha_1^{1/3} e^{2\pi i/3}.$$

Because the imaginary part of  $\alpha_1$  is positive, the complex argument of  $\beta_1$  is a little greater than  $2\pi/3$

#### 4.2.2 Outer Lindblad radius

Near  $r = R_2$ , we can approximate the solution as in the previous section. As before, we obtain a complex Airy's equation

$$\partial_r^2 u + \epsilon^2 \alpha_2 (r - R_2) u = 0 \quad (41)$$

where  $\alpha_2 = \partial_r f$ , evaluated at  $r = R_2$ . The solution takes the form;

$$u = a_2 \text{Ai}[\beta_2(R_2 - r)] + b_2 \text{Bi}[\beta_2(R_2 - r)], \quad (42)$$

in which  $a_2$  and  $b_2$  are two complex constants, and

$$\beta_2 = \epsilon^{2/3} \alpha_2 (-\alpha_2)^{-2/3}, \quad (43)$$

The imaginary part of  $\alpha_2$  to leading order is

$$\text{Im}(\alpha_2) = \frac{2\sigma}{\kappa_2} \left( \frac{\partial}{\partial r} \ln \left[ \frac{\kappa' + m\Omega'}{\kappa} \right] \right)_2. \quad (44)$$

It can be shown that the right hand side is negative for all  $m$  for realistic  $\kappa$  and  $\Omega$  profiles. Now,

$$\beta_2 = -\epsilon^{2/3} (-\alpha_2)^{1/3}.$$

Because the real part of  $\alpha_2$  is negative, the complex argument of  $\beta_2$  is a little less than  $-\pi$ .

#### 4.2.3 Corotation radius

When  $r$  is close to  $R_c$  we obtain the approximate equation

$$\partial_r^2 u + k_z^2 \alpha_c (r - R_c)^{-2} u = 0,$$

with

$$\alpha_c = \frac{\kappa^2}{m^2 (\Omega')^2}$$

evaluated at  $r = R_c$ . This admits a solution of the form

$$u = a_c (r - R_c)^{1/2 + \beta_c} + b_c (r - R_c)^{1/2 - \beta_c}, \quad (45)$$

where  $a_c$  and  $b_c$  are complex constants and, to leading order in large  $\epsilon$ ,

$$\beta_c = \epsilon (-\alpha_c)^{1/2}. \quad (46)$$

We denote this solution hereafter by  $u_c$ .

The imaginary part of  $\alpha_c$  to leading order in small  $\sigma$  is given by

$$\text{Im}(\alpha_c) = \frac{2\kappa_c^2 \sigma}{m^3 (\Omega'_c)^3} \left( \frac{\partial}{\partial r} \ln \left[ \frac{\kappa}{\Omega'} \right] \right)_c. \quad (47)$$

This can be demonstrated to be negative for all  $m > 0$ . Thus

$$\beta_c = i \alpha_c^{1/2} \epsilon.$$

### 4.3 Behaviour far from the resonant cavity

We require the trapped mode to decay outside its resonant cavity, which is circumscribed by  $R_1$  and  $R_2$ . By applying these two boundary conditions the two unknown constants  $b_1$  and  $b_2$  can be determined.

#### 4.3.1 The region $r < R_{1r}$

First we inspect the inner region of the disk,  $r < R_{1r}$ , far from the resonant cavity. In this region we have  $|\epsilon^{2/3}(R_1 - r)| \gg 1$  for sufficiently large  $\epsilon$ , which supplies the following asymptotic forms for the Airy functions:

$$\begin{aligned} \text{Ai}[\beta_1(R_1 - r)] &= [\beta_1(R_1 - r)]^{-1/4} \left( e^{-\xi} + i e^{\xi} \right) \\ \text{Bi}[\beta_1(R_1 - r)] &= [\beta_1(R_1 - r)]^{-1/4} \left( i e^{-\xi} + e^{\xi} \right), \end{aligned}$$

where

$$\xi = \frac{2}{3} [\beta_1(R_1 - r)]^{3/2}. \quad (48)$$

Because of Stokes phenomenon the argument of  $\beta_1(R_1 - r)$  is key and we must use (40) to choose the correct asymptotic expression<sup>1</sup>. This also tells us that  $\text{Re}(\xi) < 0$ . So in order to obtain a decaying  $u$  we must eliminate the  $\exp(-\xi)$  terms and keep the  $\exp(\xi)$  terms. This can be accomplished if  $b_1 = i a_1$ . The solution near the inner Lindblad resonance we now denote by  $u_1$  and write as

$$u_1 = a_1 \{ \text{Ai}[\beta_1(R_1 - r)] + i \text{Bi}[\beta_1(R_1 - r)] \}. \quad (49)$$

#### 4.3.2 The region $r > R_{2r}$

We turn now to the outer region of the disk far from the resonant cavity and with  $r > R_{2r}$ . Here for sufficiently large  $\epsilon$  we have  $|\epsilon^{2/3}(R_2 - r)| \gg 1$ , and the Airy functions are approximated by

$$\begin{aligned} \text{Ai}[\beta_2(R_2 - r)] &= \frac{1}{2\sqrt{\pi}} [\beta_2(R_2 - r)]^{-1/4} e^{-\zeta} \\ \text{Bi}[\beta_2(R_2 - r)] &= \frac{1}{\sqrt{\pi}} [\beta_2(R_2 - r)]^{-1/4} \left( \frac{i}{2} e^{-\zeta} + e^{\zeta} \right), \end{aligned}$$

with

$$\zeta = \frac{2}{3} [\beta_2(R_2 - r)]^{3/2}. \quad (50)$$

The correct asymptotic form follows from Eq. (44), which also tells us that  $\text{Re}(\zeta) > 0$ . To ensure decaying solutions we zero all the  $\exp(\zeta)$  terms, which corresponds simply to

<sup>1</sup> See for example <http://functions.wolfram.com/Bessel-TypeFunctions/AiryAi>.

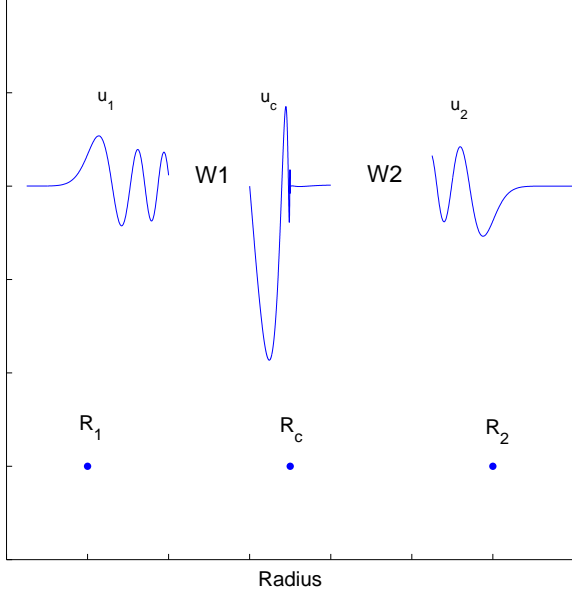


**Figure 1.** A schematic diagram of the three solutions  $u_1$ ,  $u_c$ , and  $u_2$  in their regions of validity: near the inner Lindblad, corotation, and outer Lindblad radii respectively. These are represented by  $R_1$ ,  $R_c$ , and  $R_2$ . Between the solutions are the regions  $W_1$  and  $W_2$  where the solution takes its WKB form.

$b_2 = 0$ . The solution near the outer Lindblad resonance is subsequently denoted by  $u_2$  and written as

$$u_2 = a_2 \text{Ai}[\beta_2(R_2 - r)]. \quad (51)$$

#### 4.4 WKB matching

In Fig. 1 the preceding three solutions are shown schematically, each separated from its neighbour by either region  $W_1$  or  $W_2$ . In these two regions we assume  $u$  takes its WKB form:

$$u = a_W f^{-1/4} \exp\left(i \epsilon \int f^{1/2} dr\right) + b_W f^{-1/4} \exp\left(-i \epsilon \int f^{1/2} dr\right).$$

Our task now is to extend solutions  $u_1$ ,  $u_2$ , and  $u_c$  into regions  $W_1$  and  $W_2$  using the above ansatz and then to obtain matching conditions which set  $\sigma$ .

##### 4.4.1 The $u_1$ solution in $W_1$

Suppose that  $R_1$  and  $R_c$  are sufficiently spaced (or  $\epsilon$  sufficiently large) so that  $|\epsilon^{2/3}(R_1 - r)| \gg 1$  in region  $W_1$ . The correct asymptotic form for  $u_1$  here is

$$u_1 = \frac{a_1}{\pi^{1/2}} [\beta_1(R_1 - r)]^{-1/4} \left( e^{-\xi} + i e^{\xi} \right),$$

which can be manipulated into approximate WKB form. First we treat  $r$  as a complex variable, by simply adding to

it a small imaginary component equal to  $iR_{1i}$ . Then we do the following:

$$\begin{aligned} \phi_1 &\equiv \int_{R_1}^r f^{1/2} dr, \\ &= \int_{R_1}^r [\alpha_1(r - R_1)]^{1/2} dr + \mathcal{O}[(r - R_1)^{5/2}], \\ &= i\xi \epsilon^{-1} + \mathcal{O}[(r - R_1)^{5/2}]. \end{aligned}$$

Here the path of integration is simply a straight horizontal line in the complex plane connecting  $R_1$  to  $r$ . We now have

$$u_1 \approx \tilde{a}_1 f^{-1/4} \left( e^{i\epsilon\phi_1} + i e^{-i\epsilon\phi_1} \right) \quad (52)$$

in the region  $W_1$ , where  $\tilde{a}_1$  is a new complex constant.

##### 4.4.2 The $u_2$ solution in $W_2$

Suppose that  $|\epsilon^{2/3}(R_2 - r)| \gg 1$  in region  $W_2$ . The correct asymptotic form for  $u_2$  here is

$$u_2 = \frac{a_2}{2\pi^{1/2}} [\beta_2(R_2 - r)]^{-1/4} \left( e^{-\zeta} + i e^{\zeta} \right).$$

As earlier, we treat  $r$  as a complex variable but this time add a small imaginary component equal to  $iR_{2i}$ . Next we define

$$\phi_2 \equiv \int_{R_2}^r f^{1/2} dr,$$

where the integration contour is a straight horizontal line joining  $R_2$  to  $r$ . To leading order it can be demonstrated that  $\epsilon\phi_2 = -i\zeta$  and so

$$u_2 \approx \tilde{a}_2 f^{-1/4} \left( e^{-i\epsilon\phi_2} + i e^{i\epsilon\phi_2} \right) \quad (53)$$

in region  $W_2$ .

##### 4.4.3 The $u_c$ solution in $W_1$ and $W_2$

So far our analysis has largely followed that of K02, but now we will deviate a little. The corotation radius introduces a problematic branch point in the asymptotic definition of  $u_c$  and as a consequence it is obliged to take two different WKB expressions, one in region  $W_1$  and another in region  $W_2$ . This subtlety appears to be incompletely treated in the two papers by Kato. Our approach here is relatively clunky but is unambiguous.

The  $u_c$  solution is rewritten as

$$u_c = \sqrt{r - R_c} \left( a_c e^{\beta_c \ln(r - R_c)} + b_c e^{-\beta_c \ln(r - R_c)} \right).$$

Now to account for the solution in  $W_1$  we define

$$\phi_3 = \int_{R_{cr} + iR_{1i}}^r f^{1/2} dr,$$

where the contour is the straight line connecting the point  $R_{cr} + iR_{1i}$  to  $r$  in the region  $W_1$ . Here  $r$  has taken the small imaginary component  $iR_{1i}$ . It can be shown to leading order in region  $W_1$

$$i\epsilon\phi_3 = -\beta_c \ln(r - R_c) + \epsilon\alpha_c^{1/2} [i \ln(i\Delta_1) - \pi],$$

where  $\Delta_1 = R_{ci} - R_{1i}$ . Note the large damping/amplification factor  $-\epsilon\pi\alpha_c^{1/2}$  which appears to have been missed in K02. In addition, in  $W_1$  we have

$$(r - R_c)^{1/2} \approx i\alpha_c^{1/4} f^{-1/4}.$$



Similarly in  $W_2$  we define

$$\phi_4 = \int_{R_{cr} + iR_{2i}}^r f^{1/2} dr.$$

The contour of integration is the straight line connecting the point  $R_{cr} + iR_{2i}$  to  $r$  in the region  $W_2$ . Here, however,  $r$  has taken a small imaginary component  $iR_{2i}$ . To leading order

$$i\epsilon\phi_4 = \beta_c \ln(r - R_c) - \epsilon\alpha_c^{1/2} i \ln(-i\Delta_2),$$

with  $\Delta_2 = R_{ci} - R_{2i}$ . For  $r$  in  $W_2$ ,

$$(r - R_c)^{1/2} \approx \alpha_c^{1/4} f^{-1/4}.$$

In summary, the WKB solution in region  $W_1$  is

$$u_c \approx i f^{-1/4} \left\{ \tilde{a}_c \exp(\epsilon\sqrt{\alpha_c}[i \ln(i\Delta_1) - \pi] - i\epsilon\phi_3) + \tilde{b}_c \exp(-\epsilon\sqrt{\alpha_c}[i \ln(i\Delta_1) - \pi] + i\epsilon\phi_3) \right\}. \quad (54)$$

The WKB solution in region  $W_2$  is

$$u_c \approx f^{-1/4} \left\{ \tilde{a}_c \exp(i\sqrt{\alpha_c}\epsilon \ln(-i\Delta_2) + \epsilon\phi_4) + \tilde{b}_c \exp(-i\sqrt{\alpha_c}\epsilon \ln(-i\Delta_2) - i\epsilon\phi_4) \right\}. \quad (55)$$

#### 4.4.4 Asymptotic matching

First the two solutions (52) and (54) are compared in region  $W_1$ . We define

$$\Psi_1 \equiv \int_{R_1}^{R_{cr} + iR_{1i}} f^{1/2} dr = \phi_1 - \phi_3$$

and then equate coefficients of  $\exp(i\epsilon\phi_1)$  and of  $\exp(-i\epsilon\phi_1)$ . This yields the two constants  $\tilde{a}_c$  and  $\tilde{b}_c$  in terms of  $\tilde{a}_1$ , which without loss of generality we let equal to 1. We have, as a consequence,

$$\tilde{a}_c = \exp \left\{ \epsilon\alpha_c^{1/2} [\pi - i \ln(i\Delta_1)] - i\epsilon\Psi_1 \right\}, \quad (56)$$

$$\tilde{b}_c = -i \exp \left\{ -\epsilon\alpha_c^{1/2} [\pi - i \ln(i\Delta_1)] + i\epsilon\Psi_1 \right\}. \quad (57)$$

Now we compare solutions (53) and (55) in region  $W_2$ . We define

$$\Psi_2 \equiv \int_{R_{cr} + iR_{2i}}^{R_2} f^{1/2} dr = \phi_4 - \phi_2,$$

and equate coefficients of  $\exp(i\epsilon\phi_2)$  and  $\exp(-i\epsilon\phi_2)$ . With Eqs (56) and (57) we obtain two equations, one which gives us  $\tilde{a}_2$  and finally the eigenvalue equation for  $\omega$ . Once  $\tilde{a}_2$  has been eliminated and, after some algebraic manipulation, the eigenvalue equation takes the form

$$\Psi_1 - \Psi_2 + \alpha_c^{1/2} \left[ \ln \left( \frac{-\Delta_1}{\Delta_2} \right) + i\pi \right] = \pi n \quad (58)$$

where  $n$  is some integer. In the next subsection we attempt to solve this equation approximately.

### 4.5 Approximate solution to the eigenvalue equation

For perhaps all realistic  $\kappa$  and  $\Omega$ , the integral functions  $\Psi_1$  and  $\Psi_2$  cannot be computed analytically. Instead, following K02 and K03a, we obtain approximations by using the asymptotic forms of  $f$  near  $R_1$ ,  $R_2$ , and  $R_c$ . Doing so certainly introduces some level of error, though the essential qualitative points we make should remain unaltered.

The  $\Psi_1$  integral is decomposed as follows

$$\begin{aligned} \Psi_1 &= \int_{R_1}^{R_{cr} + iR_{1i}} f^{1/2} dr, \\ &= \int_{R_1}^{R_3} f^{1/2} dr + \int_{R_3}^{R_{cr} + iR_{1i}} f^{1/2} dr, \end{aligned}$$

where  $R_3$  is an intermediate point on the line connecting  $R_1$  and  $R_{ci} + iR_{1i}$ . In the first integral we approximate  $f$  by its asymptotic form near  $R_1$ , i.e.  $f = \alpha_1(r - R_1)$ , while in the second we use its form near  $R_c$ ,  $f = \alpha_c(r - R_c)^{-2}$ . The integrals are then straightforward to calculate and we find

$$\Psi_1 \approx \frac{2}{3} \alpha_1^{1/2} (R_{3r} - R_{1r})^{3/2} + \alpha_c^{1/2} \ln \left( \frac{R_c - R_3}{i\Delta_1} \right).$$

An analogous procedure furnishes us with

$$\Psi_2 \approx -\frac{2}{3} (-\alpha_2)^{1/2} (R_{2r} - R_{4r})^{3/2} + \alpha_c^{1/2} \ln \left( \frac{R_4 - R_c}{-i\Delta_2} \right),$$

where we have introduced the intermediate point  $R_4$  which lies on the line connecting  $R_2$  and  $R_{cr} + iR_{2i}$ .

With these expressions, the eigenvalue equation (58) becomes the more manageable

$$\begin{aligned} \frac{2}{3} \alpha_1^{1/2} \Delta R_1^{3/2} + \frac{2}{3} (-\alpha_2)^{1/2} \Delta R_2^{3/2} \\ + i\alpha_c^{1/2} \pi + \alpha_c^{1/2} \ln \left( \frac{\Delta R_3 + i\Delta_1}{\Delta R_4 - i\Delta_2} \right) = \pi n, \end{aligned} \quad (59)$$

where

$$\begin{aligned} \Delta R_1 &= R_{3r} - R_{1r}, & \Delta R_2 &= R_{2r} - R_{4r}, \\ \Delta R_3 &= R_{cr} - R_{3r}, & \Delta R_4 &= R_{4r} - R_{cr}. \end{aligned}$$

Next we use the assumption that  $\sigma$  is small and expand  $\alpha_1$ ,  $\alpha_2$ ,  $\alpha_c$  in powers of  $\sigma$ ,

$$\begin{aligned} \alpha_1 &= \alpha_{11} + \alpha_{12} i\sigma + \mathcal{O}(\sigma^2), \\ -\alpha_2 &= \alpha_{21} + \alpha_{22} i\sigma + \mathcal{O}(\sigma^2), \\ \alpha_c &= \alpha_{c1} + \alpha_{c2} i\sigma + \mathcal{O}(\sigma^2), \end{aligned}$$

where the  $\alpha$  coefficients on the right sides are all real and positive except for  $\alpha_{c2}$ , (see Section 4.2). Note that K02 neglects these higher order corrections in the analogous terms of his analysis; however, these corrections will be important in the imaginary component of Eq. (59). We next take the imaginary part of Eq. (59) but neglect the last term on the left side. This term contributes terms proportional to  $\sigma \ln(\Delta R_1/\Delta R_2)$ ,  $\sigma/\Delta R_1$ , and  $\sigma/\Delta R_2$  all of which will be subdominant to the other terms if  $R_1$ ,  $R_2$ , and  $R_c$  are sufficiently well separated so that the  $\Delta R_i$  are large and of the same order. Finally, we can solve for  $\sigma$ ,

$$\sigma = \frac{-3\pi\alpha_{c1}^{1/2}}{\alpha_{12}\alpha_{11}^{-1/2}\Delta R_1^{3/2} + \alpha_{22}\alpha_{21}^{-1/2}\Delta R_2^{3/2}}. \quad (60)$$

Thus  $\sigma$  is negative.

However, a negative  $\sigma$  contradicts the initial assumption that  $\sigma > 0$  (so crucial in negotiating the Stokes phenomenon). If, on the other, hand we begin the analysis with the assumption  $\sigma < 0$  we finish with the opposite result:  $\sigma$  must be positive. The only resolution to the impasse is to take  $\sigma = 0$ . But this means that the modes will possess undefined derivatives. The conclusion is that there exist no trapped 3D normal modes for such WKB waves.

Before we continue, it should be noted that the negative results of Sections 3 and 4 and Appendix A pertain to specific cases associated with certain approximations: e.g. the local shearing sheet model and incompressible and slightly incompressible fluids, and when in a more realistic geometry, the WKB limit of large  $k_z$ . They are hence not proofs for the non-existence of *all* trapped 3D inertial waves near corotation. Together these results, however, offer a good argument that this is indeed the case.

## 5 SHEARING WAVES AND THE CONTINUOUS SPECTRUM

In this section we briefly demonstrate the dynamical behaviour of the continuous spectrum introduced in the shearing sheet analysis of Section 3. This is accomplished by inverting the temporal Fourier transform,

$$U(x, t) = \int_{\Gamma} u(x, \omega) e^{-i\omega t} d\omega, \quad (61)$$

where  $u(x, \omega)$  is the solution to the modal problem and  $\Gamma$  is the appropriate integration contour in the complex  $\omega$  plane. It is assumed that  $\omega$  is real except near any singularity, at which point the integration path  $\Gamma$  will deviate above the singularity.

For a typical initial value problem, in which the initial condition is stipulated, we would construct  $u$  using a Greens function. Usually such problems throw up complicated integrals that are difficult to solve, and the analysis is usually limited to the large time asymptotic regime (Booker and Bretherton 1967, Watts et al. 2004, for example). In Appendix C we undertake such an analysis and show that localised initial conditions evolve towards decaying shearing inertial waves (for a description of shearing waves see Johnson and Gammie 2005, Balbus and Hawley 2006). This long time behaviour issues from the collective influence of the corotation singularities. To emphasise this point, we present a slightly different calculation below in which each member of the continuous spectrum is summed equally. Doing so allows the inversion integral to be solved analytically and thus compared with the exact shearing wave solution of Johnson and Gammie (2005).

### 5.1 Shearing waves

Let us start with the integral (61) and immediately change the integration variable to

$$\theta = k_{\perp} x + \frac{k_{\perp} \omega}{q\Omega k_y}. \quad (62)$$

This is identical to the  $x^*$  introduced earlier, but in the following it is denoted differently in order to avoid confusion with  $x$ . The new coordinate measures the distance between  $x$  and the corotation point specified by  $\omega$ . In addition, a dimensionless time coordinate is introduced

$$\tau = \left( \frac{q\Omega k_y}{k_{\perp}} \right) t \quad (63)$$

We hence obtain

$$U = \left( \frac{q\Omega k_y}{k_{\perp}} \right) e^{i k_x(t)x} \int_{\tilde{\Gamma}} \hat{u}(x, \theta) e^{-i\tau\theta} d\theta, \quad (64)$$

where  $\tilde{\Gamma}$  is a contour in  $\theta$  space,  $u(x, \omega) = \hat{u}(x, \theta)$ , and the time-dependent (shearing) radial wavenumber is

$$k_x(t) = q\Omega k_y t.$$

A simple shift in time introduces a constant  $k'_x$  into the above expression, and will render  $k_x(t)$  in the familiar form used in Balbus (2003). The integral (61) now represents not a sum over all the  $\omega$  but, for a given  $x$  location, a sum over all the corotation points that influence the dynamics.

Before we specify the form of  $u$  the basic structure of the solution should be appreciated. First, we have a shearing wave contribution from the  $\exp[ik_x(t)x]$ . Second, this spatial dependence will be modulated by a possible  $x$ -dependent factor issuing from the integral in (64), the details of which are linked to the initial condition. This integral will also set the time-dependence of the solutions' amplitude. For large times the amplitude decays like  $t^{-3/2 \pm \nu}$  (just as in Booker and Bretherton 1967). The dominant contributions to the integral in this case come from the combined critical radii (the corotation points).

To better clarify the action of the continuous spectrum, we treat an equal sum of its component singular modes; there is hence no modulation arising from localised initial conditions. Consequently, we set  $\hat{u}(x, \theta) = u_s(\theta)$ , where  $u_s$  is defined in Eq. (25). Now the spatial structure of the solution becomes a pure shearing wave with the integral in Eq. (64) depending on time only through  $\tau$ . We let this integral equal the amplitude function  $A(\tau)$ , which we now calculate. The amplitude function involves a linear combination of the two integrals:

$$\begin{aligned} A_1 &= \int_0^{\infty} \sqrt{\theta} [I_{\nu}(\theta) - I_{-\nu}(\theta)] e^{-i\tau\theta} d\theta, \\ A_2 &= \int_{-\infty}^0 \sqrt{\theta} [I_{\nu}(\theta) + e^{2\pi i\nu} I_{-\nu}(\theta)] e^{-i\tau\theta} d\theta. \end{aligned}$$

Both integrals are proportional to

$$\int_0^{\infty} \sqrt{\theta} K_{\nu}(\theta) e^{-i\tau\theta} d\theta,$$

which can be evaluated in closed form in terms of hypergeometric functions (Gradshteyn and Ryzhik 1963). Finally, after some tedious algebraic manipulation using a chain of functional identities, one can express the time-dependent amplitude of the shearing wave as

$$\begin{aligned} A(\tau) &= c_1 F\left(\frac{3}{4} - \frac{1}{2}\nu, \frac{3}{4} + \frac{1}{2}\nu; \frac{1}{2}; -\tau^2\right) \\ &\quad + d_1 \tau F\left(\frac{5}{4} - \frac{1}{2}\nu, \frac{5}{4} + \frac{1}{2}\nu; \frac{3}{2}; -\tau^2\right), \end{aligned}$$

where  $c_1$  and  $d_1$  are two constants and  $F(a, b, c; z)$  is a Gauss hypergeometric function, often represented as  ${}_2F_1$ . This amplitude is exactly that of a pure shearing wave computed directly from the governing equation (8) rendered in shearing coordinates:

$$\partial_{\tau}^2 A + \beta^2(1 + \tau^2)^{-1} A = 0, \quad (65)$$

(for the derivation see Johnson and Gammie 2005 or Balbus and Hawley 2006).

The main point to take away is that inertial shearing waves are equivalent to the continuous spectrum issuing from the corotation singularities. This simple relationship

has not been generally appreciated in the astrophysics community, but is quite natural (Craik and Criminale, 1986). A shearing wave understood this way is but a sum of structures  $u_s$  each tightly localised to its critical radius and convected perfectly upon the background shear, like tracers.

## 6 INSTABILITY IN A SLENDER TORUS

The previous sections have investigated the role of the corotation point in an extended disk. The analysis was local and the disk-boundaries were sent to infinity. Consequently, trapped modes could not arise. In this section a different scenario is attacked: an inviscid slender torus, the radial boundaries of which play the essential part. Specifically, we examine the effect the corotation point has upon the incompressible three-dimensional Papaloizou-Pringle instability (Papaloizou and Pringle 1984, 1985, Drury 1985, Goldreich et al. 1986).

The classical model of this global hydrodynamical instability is two-dimensional, in which case the corotation point is not a singularity of the governing equations. The mechanism of instability proceeds in this case from the efficient communication of angular momentum from the inner boundary to the outer via wave motions across the corotation point. If, however, the mode in question possesses vertical structure, the corotation point, being singular, will impede this transfer and either inhibit growth or prohibit the formation of normal modes entirely (as in the previous sections). In the following we characterise this phenomenon for general  $q$ . Note that our results complement those obtained by Sternberg et al. (2008) who examine a similar problem with fixed boundary walls.

### 6.1 Mathematical set-up

We consider the shearing sheet approximation to a narrow incompressible fluid annulus with no equilibrium vertical structure. The centre of the sheet is anchored at the centre of the annulus  $r_0$  so that the fluid occupies the radial region circumscribed by  $|x| \leq s$ , where  $2s$  is the total radial width of the annulus. The Eulerian perturbation equations are Eqs (4)-(7), and we draw our general solution for  $u'_x$  for a given  $(k_y, k_z, \omega)$  mode from Eq. (9).

The appropriate boundary conditions for a narrow annulus is that the Lagrangian enthalpy perturbation must vanish at the free surfaces  $x = \pm s$ . This condition may be represented by

$$h' + \Delta x \frac{dh_0}{dx} = 0, \quad (66)$$

where

$$\Delta x = \frac{i u'_x}{q \Omega k_y x + i \sigma}$$

is the radial displacement at the boundary. The Eulerian enthalpy perturbation is supplied by

$$h' = \frac{i \tilde{\omega}}{k_\perp^2} \partial_x u'_x + i(2 - q) \Omega \frac{k_y}{k_\perp^2} u'_x,$$

and the radial gradient of the equilibrium enthalpy  $h_0$  is

$$\frac{dh_0}{dx} = -(2q - 3) \Omega^2 x.$$

This enthalpy gradient aids gravity negate the centrifugal force when the rotation law is non-Keplerian.

In this section we consider modes that are corotating with the centre of the annulus, so that  $\omega_r = 0$ , but which possess nonzero  $\sigma$ . We also scale space by  $k_\perp^{-1}$  as in Section 2.3, while introducing the scaled growth rate

$$\bar{\sigma} = \frac{k_\perp}{q k_y} \left( \frac{\sigma}{\Omega} \right),$$

(which in Section 2.3 is equal to  $-x_c$ ). The boundary condition can now be expressed neatly as

$$q^2 (x + i \bar{\sigma})^2 \frac{du'_x}{dx} + \{q(2 - q)(x + i \bar{\sigma}) - (2q - 3)(1 + k_z^2/k_y^2)x\} u'_x = 0, \quad (67)$$

which must hold at  $x = \pm s$ . The expression for  $u'_x$  is

$$u'_x = A \sqrt{x + i \bar{\sigma}} I_\nu(x + i \bar{\sigma}) + B \sqrt{x + i \bar{\sigma}} I_{-\nu}(x + i \bar{\sigma}),$$

where  $A$  and  $B$  are constants to be determined, and  $\nu$  can be computed from (16). Once  $A$  and  $B$  are eliminated from the two equations we arrive upon the dispersion relation for  $\bar{\sigma}$ , which is a function of the three dimensionless parameters,  $q$ ,  $k_z/k_y$ , and  $s$ .

### 6.2 Growth rates

Unfortunately, the dispersion relation is transcendental in  $\bar{\sigma}$ . In the interest of readability, the full expression is banished to Appendix D. In general, the growth rates must be computed numerically. Nevertheless, some analytic progress can be made if it is assumed that the width of the annulus is small relative to the typical lengthscale of a  $(k_y, k_z)$  mode, i.e.  $|s| \ll 1$ . If the annulus was much wider, especially if the mode's Lindblad resonances fitted into the domain, communication between the two boundaries via incompressible motions would fail and the instability would evaporate. In addition, we let the growth rates scale as  $\bar{\sigma} \sim s$  (Balbus, 2003). This permits the scaling  $I_\nu(i \bar{\sigma} \pm s) \sim s^\nu$ , which helps us fish out the most significant terms in the dispersion relation. To leading order it can then be boiled down to

$$2q^2(2 - q) f(\sigma_1) \sigma_1^2 + 2q^2 i (2q - 3) \nu g(\sigma_1) \sigma_1 + f(\sigma_1) \left[ 3(3 - q^2) + \frac{k_z^2}{k_y^2} (3 - 2q)^2 \right] = 0, \quad (68)$$

where we have set  $\bar{\sigma} = s \sigma_1 + \mathcal{O}(s^2)$  and where

$$f(\sigma_1) = (i \sigma_1 - 1)^{2\nu} - (i \sigma_1 + 1)^{2\nu},$$

$$g(\sigma_1) = (i \sigma_1 - 1)^{2\nu} + (i \sigma_1 + 1)^{2\nu}.$$

Though the reduced dispersion relation cannot be solved analytically for  $\sigma_1$ , it yields two significant results.

First, we can establish the two-dimensional stability criterion easily. By setting  $k_z = 0$ , and consequently  $\nu = 1/2$ , we get the twinned growing and decaying modes

$$q \sigma_1 = \pm \sqrt{3(q^2 - 3)}$$

in agreement with Papaloizou and Pringle (1985) (see also Balbus 2003). The instability criterion is thence  $q > \sqrt{3}$ .

Second, it yields the curve of marginal stability for general three-dimensional modes once we set  $\sigma_1 = 0$ . The curve is described by

$$q_{\text{crit}} = \frac{3}{4(k_z/k_y)^2 - 3} \left( 2(k_z/k_y)^2 - \sqrt{3 - (k_z/k_y)^2} \right). \quad (69)$$

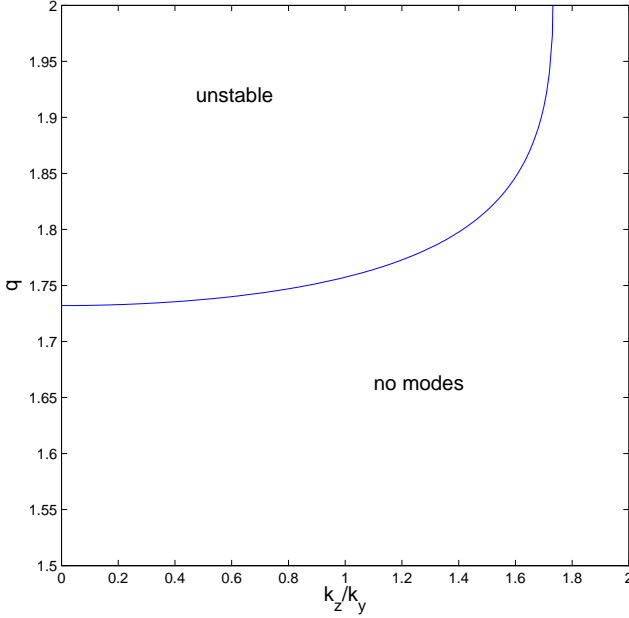


**Figure 2.** The marginal stability curve in the parameter space  $(k_z/k_y, q)$  given by (69). The region above it is unstable. The region bounded by it and the vertical  $k_z/k_y = 0$  axis circumscribe parameters for which no modes exist.

The curve of critical  $q$  as a function of  $k_z/k_y$  is plotted in Fig. 2. There we can see clearly that the greater the vertical pitch of the wavevector, the greater the critical  $q$  necessary for instability.

As expected, the most unstable modes are two-dimensional. Three-dimensional modes, on the other hand, must contend with the singularity at corotation  $x = 0$ , which interferes with the mechanism of instability. As discussed in Section 2.4, waves with small wavevector pitch,  $k_z/k_y \leq q\Omega/(2\kappa)$  (i.e.  $\beta \leq 1/2$ ), pick up a phase shift upon crossing this point. But the singularity is far more destructive for modes with greater pitch,  $k_z/k_y > q\Omega/(2\kappa)$  (i.e.  $\beta > 1/2$ ) which are severely damped. No normal modes (growing or otherwise) of the latter class are possible in the slender torus. This is also true for some low  $k_z/k_y$  modes which only suffer the phase shift. Generally, however, such  $\beta \leq 1/2$  modes do exist and occur as growing/decaying pairs. They are situated in the region above the marginal curve in Fig. 2. Their growth rates are lower than the equivalent 2D mode at the same  $q$  because the phase shift renders the transfer of angular momentum across corotation less inefficient. This is illustrated particularly well in the eigenfunction profiles in the next subsection.

### 6.3 Eigenfunctions

To examine the effect of the corotation singularity on the structure of the unstable modes we fix  $q = 1.8$  and  $s = 0.1$  and subsequently vary the ratio  $k_z/k_y$  from 0 to the value at which modes cease to exist (near 1.5). The eigenproblem Eq. (D1) is solved numerically by a Newtown-Raphson method.

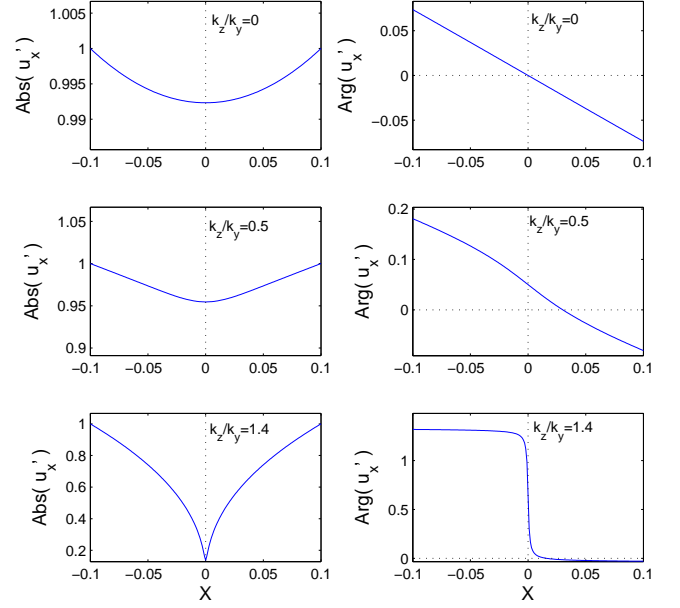


**Figure 3.** The modulus and argument of the  $u'_x$  eigenfunction's radial structure for  $q = 1.8$ ,  $s = 0.1$ , and various  $k_z/k_y$ . Panels (a) and (b) show the (two-dimensional) eigenfunction when  $k_z/k_y = 0$ . The growth rate here is  $\sigma = 7.60 \times 10^{-2} \Omega$ . Panels (c) and (d) show the case when  $k_z/k_y = 0.5$ . Note that the presence of the corotation singularity breaks the radial symmetry. As a consequence, the unscaled growth rate is less: we compute  $\sigma = 6.23 \times 10^{-2} \Omega$ . Finally, panels (e) and (f) show an eigenfunction with  $k_z/k_y = 1.4$ , a value which positions the mode very near the stability boundary sketched in Fig. 3. The unscaled growth rate is  $\sigma = 9.91 \times 10^{-4} \Omega$ . Note the near discontinuity in the argument at corotation. Motions on either side of this point are out of phase by a quantity near  $\pi/2$ , and thus the transfer of angular momentum and energy from the inner boundary to the outer is severely impeded. The eigenfunctions are normalised so that the maximum of  $|u'_x|$  is 1.

In Fig. 3, the top two panels (a) and (b) exhibit the Eulerian radial velocity component ( $u'_x$ ) of the classical two-dimensional mode ( $k_z = 0$ ) as a function of dimensionless  $x$ . Both the modulus and argument are presented. The most important features here are the relatively small variation in radius ( $x$ ), which is of order  $s^2$ , and particularly the small change in phase from the inner edge to the outer edge.

In the next two panels, Figs 3c and 3d, a three-dimensional mode is plotted with  $k_z/k_y = 0.5$ . The mode grows slower than the previous case, and the symmetry of its structure is broken. In Figs 3e and 3f the  $k_z/k_y = 1.4$  case is presented, which is near criticality. Any value of  $k_z/k_y$  much larger does not return a modal solution. The salient feature here is the near discontinuity in  $\text{Arg}(u'_x)$  at the corotation radius. Motions on either side of this point are out of phase by a quantity that approaches  $\pi/2$ . This represents the limit of severe damping of energy and angular momentum transfer and thus zero growth.

## 7 CONCLUSION

Axisymmetric inertial waves can become trapped in the inner regions of disks orbiting black holes, forming standing modes (Okazaki et al. 1987). In certain cases a small set of non-axisymmetric inertial waves can do the same (Perez et al. 1997). However, most 3D non-axisymmetric inertial waves possess a corotation singularity within their resonant cavity and, as a consequence, these waves will have difficulty forming trapped standing motions.

This idea was demonstrated with a simple local model, the shearing sheet, which crystallises the important physical and mathematical points thus allowing a straightforward interpretation of the problem. Its conclusions are bolstered by a WKB analysis in a more realistic semi-global model in cylindrical geometry in Section 4, and a compressible analysis in Appendix A. The central point is that a trapped standing wave must carefully balance its two component travelling waves in order to satisfy the two decaying boundary conditions far away from the corotation region; at the very least, these two travelling waves must possess comparable amplitudes. But the corotation singularity acts as a powerful wave absorber, heavily damping one of the waves relative to the other and hence destroying the necessary balance. If one boundary condition is satisfied the other must be violated.

In summary, non-axisymmetric 3D inertial waves should play little direct role in QPO models based on diskoseismology, though they may be implicated in parametric instabilities, where they can act as ‘intermediaries’ transferring energy between two trapped axisymmetric waves (for example, Ferreira and Ogilvie 2008). More generally, the viability of diskoseismology rests on the interactions between trapped inertial waves and their turbulent environment. Recent local and global simulations, in particular, have shown that trapped modes struggle to emerge from MRI-induced turbulence (Arras et al. 2006, Reynolds and Miller 2009).

The corotation singularity, while forbidding discrete normal modes, on the other hand generates a continuous set of neutral singular ‘modes’, a continuous spectrum. We show that an ensemble of these singular structures corresponds exactly to the inertial shearing waves computed by Johnson and Gammie (2005) and Balbus and Hawley (2006), and in Appendix C we use them to solve the initial value problem for localised initial conditions in the asymptotic limit of large time. This provides an alternative, and analytically tractable, interpretation which helps deepen our understanding of shearing waves, which appear naturally in shearing box simulations and may be important in planet-disk interactions (Balbus 2003, Balbus and Hawley 2006, Shen et al. 2006).

Lastly, unstable 3D modes in a simple model of a slender torus were studied in the context of corotational damping. As expected, 3D modes of small pitch  $k_z/k_y$  grow at slower rate than their 2D counterparts on account of the impeded angular momentum transfer at the corotation radius, which is a singularity when  $k_z \neq 0$ . Modes of greater pitch do not exist at all. This simple example analysis fleshes out rather nicely the ideas put forward in Li et al. (2003). Moreover, it shows that astrophysical tori which are unstable to the incompressible Papaloizou and Pringle instability will be dominated by the two-dimensional unstable modes above all others.

## ACKNOWLEDGEMENTS

The authors would like to thank the anonymous reviewer for helpful comments which much improved the paper. H. N. L. thanks Christopher Heaton for helpful and encouraging advice on the continuous spectrum, and also to Gordon Ogilvie who pointed out important flaws in our treatment of viscosity in an earlier draft. This work has been supported by a grant from the Conseil Régional de l’Île de France.

## REFERENCES

- Abramowitz, M., Stegun, I. A., 1972. *Handbook of Mathematical Functions*, Dover Press, New York.
- Abramowicz, M. A., Kluźniak, W., 2001. A&A, 371, L19.
- Arras, P., Blaes, O., Turner, N. J., 2006. ApJ, 645, L65.
- Balbus, S. A., 2003. ARA&A, 41, 555.
- Balbus, S. A., Hawley, J. F., 2006. ApJ 652, 1020.
- Booker, J. R., Bretherton, F. P., 1967. JFM, 27, 513.
- Case, K. M., 1960. PhFl, 3, 143.
- Craik, A. D. D., Criminale, W. O., 1986. RSPSA, 406, 13.
- Drazin, P. G., 2002. *Introduction to Hydrodynamical Stability*, Cambridge Univ. Press, Cambridge.
- Drury, L. O’C., 1985. MNRAS, 217, 821.
- Ferreira, B. T., Ogilvie, G. I., 2008. MNRAS, 386, 2297.
- Goldreich, P., Lynden-Bell, D., 1965. MNRAS, 130, 125.
- Goldreich, P., Goodman, J., Narayan, R., 1986. MNRAS, 221, 339.
- Gradshteyn, I. S., Ryzhik, I. M., 1963. *Table of Integrals, Series, and Products*, Academic Press, London.
- Johnson, B. M., Gammie, C. F., 2005. ApJ, 626, 978.
- Kato, S., 1990. PASJ, 42, 99.
- Kato, S., 2001a. PASJ, 53, 1.
- Kato, S., 2001b. PASJ, 53, L37.
- Kato, S., 2002. PASJ, 54, 39.
- Kato, S., 2003a. PASJ, 55, 257.
- Kato, S., 2003b. PASJ, 55, 801.
- Korycansky, D. G., Pringle, J. E., 1995. MNRAS, 272, 618.
- Li, H., Finn, J. M., Lovelace, R. V. E., Colgate, S. A., 2000. ApJ, 533, 1023.
- Li, L.-X., Goodman, J., Narayan, R., 2003. ApJ, 593, 980.
- Lovelace, R. V. E., Li, H., Colgate, S. A., Nelson, A. F., 1999. ApJ, 513, 805.
- McClintock, J. E., Remillard, R. A., 2003. In *Compact Stellar X-ray Sources* (eds. Lewin W. H. G. and van der Klis, M.) Cambridge Univ. Press, Cambridge.
- Ogilvie, G. I., 1998. MNRAS, 297, 291.
- Okazaki, A. T., Kato, S., Fukue, J., 1987. PASJ, 39, 457.
- Papaloizou, J. C. B., Pringle, J. E., 1984. MNRAS, 208, 721.
- Papaloizou, J. C. B., Pringle, J. E., 1985. MNRAS, 213, 799.
- Perez, C. A., Silbergleit, A. S., Wagoner, R. V., Lehr, D. E., 1997. ApJ 476 589.
- Reynolds, C. S., Miller, M. C., 2009. ApJ 692, 869.
- Schmid, P. J., Henningson, D. S., 2001. *Stability and Transition in Shear Flows*, Springer, New York.
- Shen, Y., Stone, J. M., Gardiner, T. A., 2006. ApJ, 653, 513.
- Sternberg, A., Umurhan, O. M., Gil, Y., Regev, O., 2008. A&A, 486, 341.

Vishniac, E. T., Diamond, P., 1989. ApJ, 347, 435.  
 Wagoner, R. V., 1999. Phys. Rep., 311, 259.  
 Watts, A. L., Andersson, N., Williams, R. L., 2004. MN-  
 RAS, 350, 927.

## APPENDIX A: DEPARTURES FROM INCOMPRESSIBILITY

This appendix reinforces the result of Section 3 by investigating the role of compressibility. The most salient effect of compressibility in our problem is the ‘leakage’ of inertial waves through the walls of their confining potential wells. We establish whether this tunneling can circumvent the strong constraints imposed by the boundary conditions and consequently permit trapped normal mode solutions. Recently Ferreira and Ogilvie (2008) numerically demonstrated that a trapped axisymmetric inertial mode can tunnel through its confining barrier and emerge on its other side as a small-amplitude p-mode. The effect seems small but may be important in the normal mode formation (or, rather, non-formation).

In light of this we undertake a generalisation of the analysis of Section 3 to a ‘slightly incompressible’ fluid; that is, we define a small parameter associated with the sound speed and expand to its first order. The incompressible analysis of the main paper is subsequently interpreted as the zeroth order approximation. As before, we attempt to describe trapped normal r-modes but again we find that no such solutions exist.

### A1 Governing equations

We return to the set of linearised equations for a small disturbance but now use the full continuity equation

$$\partial_t \rho + \mathbf{u} \cdot \nabla \rho = -\rho \nabla \cdot \mathbf{u},$$

instead of the incompressibility restriction  $\nabla \cdot \mathbf{u} = 0$  and we assume an ideal fluid, so that  $p = c_s^2 \rho$ , where  $c_s$  is the (constant) sound speed. In addition, the tidal potential  $\Phi$  picks up a component representing vertical gravity.

The vertical equilibrium of the basic state exhibits a Gaussian vertical structure. Consequently, we assume a mode structure proportional to

$$\exp(ik_y y - i\omega t) \text{He}_n[z/(\sqrt{2}H)],$$

where  $\text{He}_n$  is a Hermite polynomial of order  $n$  and  $H = c_s/\Omega$  is the disk scale height. In the shearing sheet model this ansatz yields the linearised equations,

$$i\tilde{\omega} h' = c_s^2 [\partial_x u'_x + ik_y u'_y + i(k_z^2/\tilde{\omega}) h'], \quad (\text{A1})$$

$$i\tilde{\omega} u'_x = -2\Omega u'_y + \partial_x h', \quad (\text{A2})$$

$$i\tilde{\omega} u'_y = \frac{1}{2}(\kappa^2/\Omega) u'_x + ik_y h', \quad (\text{A3})$$

in which we have defined  $k_z \equiv \sqrt{n}/H$ , and eliminated  $u'_z$ . This set of equations can be combined to form an equation for  $u'_x$ ,

$$\partial_x^2 u'_x + \frac{2q\Omega \tilde{\omega} k_y}{c^2 k_\perp^2 - \tilde{\omega}^2} \partial_x u'_x + \left\{ k_\perp^2 \left( \frac{\kappa^2}{\tilde{\omega}^2} - 1 \right) \left( 1 - \frac{\tilde{\omega}^2}{c^2 k_\perp^2} \right) - \frac{\kappa^2 k_y^2}{\tilde{\omega}^2} + \frac{q\kappa^2 k_y}{c^2 k_\perp^2 - \tilde{\omega}^2} \right\} u'_x = 0.$$

This equation exhibits both the regular singular point at corotation,  $\tilde{\omega} = 0$ , and the apparent singularities at the vertical resonances,  $\tilde{\omega}^2 = c_s^2 k_\perp^2$ . The latter points, with the Lindblad resonances  $\tilde{\omega}^2 = \kappa^2$ , circumscribe the two potential barriers. We set  $\omega = \omega_r + i\sigma$  and change coordinates as in Section 2. Doing so introduces the new dimensionless parameter

$$\delta = (H k_\perp)^{-1},$$

which measures the importance of compressible effects. To make further progress the key step is to assume this quantity is small and to expand the mode equation in its powers. The result up to order  $\delta^2$  is

$$\partial_x^2 u + 2\delta^2 \alpha^2 X \partial_x u + \left\{ \frac{\beta^2}{X^2} - (1 - \gamma) + \alpha^2 X^2 \right\} u = 0, \quad (\text{A4})$$

where  $X = x - ix_c$ , with  $\beta$  and  $x_c$  given in Section 2, and

$$\alpha = q(k_y/k_\perp) \delta, \quad \gamma = \delta^2 \kappa^2 [q(k_y/k_\perp)^2 - 1].$$

Note that we have dropped the prime and subscript  $x$  on  $u'_x$ . In addition, we could expand  $u$  in small  $\delta$  as well, but we retain all its subdominant components.

The equation (A4) is governed by the dimensionless parameters  $q$ ,  $k_y/k_z$ , and  $\delta$ . By setting  $\delta = 0$  we recover Bessel’s equation (12). The additional terms alter the nature of the potential, which is described by the negative of the term in curly brackets. To leading order, the two forbidden zones are contained, on the one hand, between  $x = \beta$  and  $x = \alpha^{-1}$ , and, on the other, between  $x = -\beta$  and  $x = -\alpha^{-1}$ . In the incompressible limit we have  $\delta \rightarrow 0$  and find the barriers extend to infinity, as in Sections 2 and 3. There are thus three zones in which wave-motion can take place. Modes localised primarily to the two regions  $|x| > \alpha^{-1}$ , far away from corotation, we identify as p-modes (density waves), and modes localised near corotation  $|x| < \beta$ , we identify as r-modes (inertial waves).

### A2 Mathematical analysis

Equation (A4) can be solved analytically by assuming the functional form

$$u = X^a e^{bX^2} f(X),$$

where  $a$  and  $b$  are constants we are free to choose. After substitution of this ansatz into (A4)  $a$  and  $b$  are set to values which zero the  $x^{-2}$  and  $x^2$  terms in the coefficient of  $f$ . The result is a version of Kummer’s equation which can be made more explicit by the coordinate transform  $Y = i\alpha\sqrt{1 - \alpha^2} x^2$ . Then we have

$$Y \partial_Y^2 f + (1 \pm \nu - Y) \partial_Y f - \eta f = 0$$

where  $\nu$  was introduced earlier in (16) and  $\eta$  is given through

$$\eta = \frac{1 \pm \nu}{2} - \frac{i(1 + \alpha^2 - \gamma)}{4\alpha\sqrt{1 - \alpha^2}}.$$

Note the ambiguity in the sign of  $\nu$  which arises from a freedom in the choice of  $a$  and which corresponds physically to the direction of the p-mode solution. Without loss of generality we take the positive sign (the left-going p-mode), but

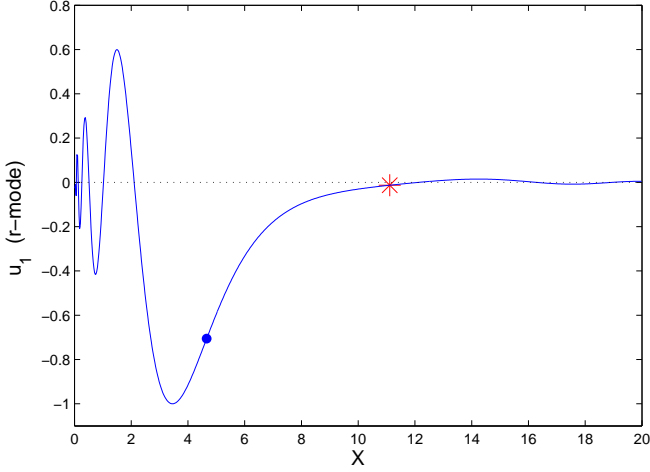


**Figure A1.** Here we present the real part of  $u_1$  for  $x > 0$  with parameters  $q = 3/2$ ,  $k_z/k_y = 7$ , and  $\delta = 0.425$ . In addition, we indicate the location of the resonances: the corotation point is at  $x = 0$ ; the solid circle refers to the Lindblad resonance,  $x = 4.67$ , and the asterisk refers to the vertical resonance,  $x = 11.1$ . The forbidden zone is hence delimited by an asterisk and a circle. We only plot  $u_1$  to identify it as possessing the features of an inertial wave. As is made clear in the text, inertial waves do not manifest as normal modes in this problem.

remain conscious that results pertaining to it also hold for the negative case (right-going mode).

The two independent solutions to Kummer's equations are  $M(\eta, \nu + 1, Y)$  and  $U(\eta, \nu + 1, Y)$ , the confluent hypergeometric functions of first and second kind respectively (Abramowitz and Stegun, 1972). The two linearly independent solutions to the original wave-shape equation (A4), with the correct values of  $a$ ,  $b$ , and  $Y$  substituted, are hence

$$u_1 = X^{1/2+\nu} \exp\left(-\frac{1}{2}\alpha^2 X^2 - \frac{1}{2}i\alpha\sqrt{1-\alpha^2}X^2\right) \times U(\eta, 1+\nu; i\alpha\sqrt{1-\alpha^2}X^2) \quad (\text{A5})$$

$$u_2 = X^{1/2+\nu} \exp\left(-\frac{1}{2}\alpha^2 X^2 - \frac{1}{2}i\alpha\sqrt{1-\alpha^2}X^2\right) \times M(\eta, 1+\nu; i\alpha\sqrt{1-\alpha^2}X^2). \quad (\text{A6})$$

We identify solution  $u_1$  with the r-mode and  $u_2$  with the (left-going) p-mode by inspection of their profiles (see Figs A1 and A2):  $u_1$  is confined almost fully to the cavity near corotation with some leakage through the potential barriers;  $u_2$  is confined to the areas outside the potential barriers with some leakage into the corotation region (which is too small to see). Both solutions decay speedily for large  $|x|$ .

### A3 Absence of trapped inertial waves

First, it is assumed that  $\sigma > 0$ . Next, consider the argument of the hypergeometric function in  $u_1$ ,

$$Y = i\alpha\sqrt{1-\alpha^2}X^2 = \alpha\sqrt{1-\alpha^2}[-2\sigma x + i(x^2 - \sigma^2)].$$

Suppose that we following the solution along  $x$  towards the corotation point from the right (in region  $x > 0$ ). When we reach  $x = \sigma$  the imaginary part of  $Y$  changes sign but the real part of  $Y$  remains negative, which means that in

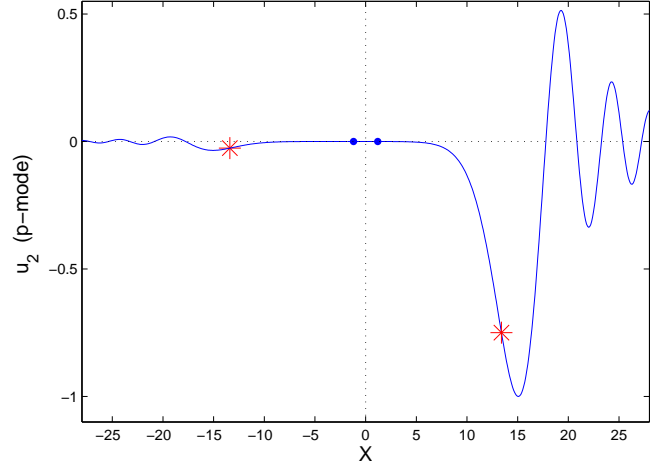


**Figure A2.** In this figure we plot the real part of the left-travelling p-mode as described by  $u_2$  as a function of  $x$ . The parameters are  $q = 3/2$ ,  $k_z/k_y = 1.75$ , and  $\delta = 0.1$ . The Lindblad resonances are at  $x = \pm 1.17$  and are denoted by solid circles, the vertical resonances at  $x = \pm 13.4$  and denoted by asterisks, and the corotation point is at  $x = 0$ .

the complex  $Y$ -plane we cross the negative real axis. But the negative real axis happens to be a branch cut for the function  $U(\eta, \nu + 1, Y)$  (Abramowitz and Stegun 1972). This means that

$$\lim_{\delta \rightarrow 0^+} U(\eta, \nu + 1, -Z + i\delta) \neq \lim_{\delta \rightarrow 0^+} U(\eta, \nu + 1, -Z - i\delta)$$

for any  $Z$  positive and real. So, in effect, when  $\sigma \neq 0$  the solution  $u_1$  exhibits a discontinuity when  $x = \sigma$  and is not analytic as a result. (In fact,  $u_1$  proceeds to a different Riemann surface.) If we set  $\sigma = 0$  then the discontinuity is removed but then the solution possesses undefined derivatives at  $x = 0$  and is thus not analytic either. Physically, the  $u_1$  is a combination of left and right-travelling p-modes, organised so that  $|u_1| \rightarrow 0$  as  $|x| \rightarrow \infty$ . But just as in Section 3, the satisfaction of these two boundary conditions comes at the price of continuity — of the function itself or its derivatives. In summary, there can be no trapped inertial modes even when compressibility is taken into account.

### A4 Density waves

On the other hand, the confluent hypergeometric  $M$  of the p-mode  $u_2$  is an entire function and thus suffers no branch cuts. If there is a small nonzero  $\sigma$  the p-mode is analytic throughout the domain: from Fig. A2 it impacts on the potential barrier from the right, decays exponentially in the forbidden region, and trickles into the narrow corotation region before emerging as a smaller amplitude p-mode oscillation on the far side of the left-most barrier. We suspect the numerical integration undertaken in the Appendix A of Li et al. (2003) produces a profile not dissimilar to  $u_2$ , though it may not capture the function's far-field decay.

**APPENDIX B: INFLUENCE OF VISCOSITY**

Typically the continuous spectrum gives rise to algebraic growth or decay. However, even a small amount of dissipation will remove the singularity at corotation, and in bounded flows the inviscid continuous spectrum will congeal into a discrete but dense set of eigenvalues each associated with a regular eigenfunction exhibiting an exponential time dependence. In the unbounded shearing sheet, however, the analogous spectrum will remain continuous and its eigenfunctions singular.

Though the singularity at corotation is removed by viscosity, an incident travelling wave should still suffer strong absorption when it strikes the corotation region. This means the arguments of Section 3, which we used to dismiss the possibility that left and right-travelling waves can be combined to form trapped standing waves, still apply qualitatively. On the other hand, one can demonstrate the impossibility of constructing a localised time-exponential solution from a sum of viscous shearing waves, and thus of viscous standing eigenmodes generally (Gordon Ogilvie, private communication). It follows that the unbounded shearing sheet must possess a viscous continuous spectrum which describes the dynamics of viscous shearing waves.

Just as in the Orr-Sommerfeld problem, the effect of a small viscosity in a disk is most pronounced at the critical radius – at corotation. A viscous boundary layer develops around this point to mediate the absorption of wave energy. From the viscous equations of motion we can derive the following sixth-order equation in the dimensionless variables of Section 2.3,

$$\Xi^2 \partial_x^2 u - \Xi^2 u + \beta^2 u = 0 \quad (\text{B1})$$

where the operator  $\Xi$  is defined by

$$\Xi = (x - ix_c) - i\mathcal{R}^{-1}(\partial_x^2 - 1), \quad (\text{B2})$$

which introduces the (modified) Reynolds number

$$\mathcal{R} = \left( \frac{q\Omega}{\nu k_\perp^2} \right) \left( \frac{k_y}{k_\perp} \right), \quad (\text{B3})$$

with  $\nu$  the kinematic viscosity. From this equation it can be shown that the internal viscous layer at corotation possesses a width of order  $\mathcal{R}^{-1/3}$  when the Reynolds number is large. Approximate solutions very close to corotation (inside the viscous layer) can be easily derived for WKBJ waves when  $\beta \sim \mathcal{R} \gg 1$ . All six solution decay (or grow) exponentially through the layer at a (spatial) rate  $(\mathcal{R}\beta)^{1/3}$ . This means the total reduction in amplitude of an incident WKBJ wave through the entire layer will be of order  $\beta^{1/3}$ , which should be contrasted with the rate  $\beta$  that emerges from the inviscid analysis of Section 2.4. Thus, viscosity allows incident waves to penetrate corotation with greater success, though the damping will still be sufficient to preclude standing eigenmodes.

**APPENDIX C: THE INITIAL VALUE PROBLEM**

This appendix offers a more formal treatment of the initial value problem than in Section 5. We return to the original linearised equations (4)-(7) and take Fourier transforms in

space and time. The temporal Fourier transform is defined by

$$\hat{f} = \int_0^\infty f e^{i\omega t} dt.$$

It follows that

$$\begin{aligned} -i\tilde{\omega}\hat{u}_x - 2\Omega\hat{u}_y &= -\partial_x\hat{h} + u_x^0, \\ -i\tilde{\omega}\hat{u}_y + \frac{\kappa^2}{2\Omega}\hat{u}_x &= -ik_y\hat{h} + u_y^0, \\ -i\tilde{\omega}\hat{u}_z &= -ik_z\hat{h} + u_z^0 \end{aligned}$$

with the incompressibility condition. It is assumed that the initial conditions,  $\mathbf{u}^0$  and  $h^0$ , are analytic and obey the far field decaying boundary conditions. Like in Section 3 this set is reduced to a single equation for  $\hat{u}_x$ . With the space dimension scaled by  $k_\perp^{-1}$  and with the transformed velocity field scaled by  $\Omega$ , we obtain

$$\partial_x^2 \hat{u}_x + \left( \frac{\beta^2}{(x - x_c)^2} - 1 \right) \hat{u}_x = \frac{1}{(x - x_c)} \Lambda(x, x_c), \quad (\text{C1})$$

where  $x_c = -(\omega k_\perp)/(q\Omega k_y)$ . Note that this definition is different to that appearing in Sections 2 and 3. Equation (C1) is the inhomogeneous Bessel's equation with

$$\Lambda(x, x_c) = \frac{i(k_\perp)}{qk_y} (\partial_x^2 u_x^0 - u_x^0) + \frac{2i}{q^2(x - x_c)} u_z^0.$$

To simplify the following mathematics, without altering our conclusions,  $u_z^0$  is set to 0. Thus  $\Lambda = \Lambda(x)$ .

**C1 Greens function solution**

Equation (C1) can be solved using a Greens function,  $G(x, y)$ , so that

$$\hat{u}_x = \int_{-\infty}^\infty \frac{\Lambda(y) G(x, y)}{y - x_c} dy,$$

in which the integration contour deviates below the singularity at  $y = x_c$ . The Greens function must satisfy the equation

$$\partial_x^2 G + \left( \frac{\beta}{(x - x_c)^2} - 1 \right) G = \delta(x - y),$$

where  $\delta(x)$  is the Dirac delta function, while at the same time satisfying the far field decaying boundary conditions. A suitable choice is

$$\begin{aligned} G(x, y) = \frac{1}{W} \{ &\Theta(y - x) \cdot u_+(y) u_-(x) \\ &+ \Theta(x - y) \cdot u_+(x) u_-(y) \}, \end{aligned}$$

where  $\Theta(x)$  is the Heaviside step function,  $u_+$  and  $u_-$  are

$$\begin{aligned} u_+ &= (x - x_c)^{1/2} K_\nu(x - x_c), \\ u_- &= (x - x_c)^{1/2} (I_\nu(x - x_c) - e^{2\pi i \nu} I_{-\nu}(x - x_c)) \end{aligned}$$

and  $W$  is their Wronskian:

$$W \equiv \left( \frac{du_+}{dx} \right) u_- - \left( \frac{du_-}{dx} \right) u_+ = (1 - e^{2\pi i \nu}).$$

We can now write down the solution to Eq. (C1),

$$\hat{u}_x = A u_- + B u_+, \quad (\text{C2})$$



where

$$A(x, x_c) = \frac{1}{W} \int_x^\infty \frac{\Lambda(y) u_+(y, x_c)}{y - x_c} dy, \quad (C3)$$

$$B(x, x_c) = \frac{1}{W} \int_{-\infty}^x \frac{\Lambda(y) u_-(y, x_c)}{y - x_c} dy. \quad (C4)$$

## C2 Evolution at large times

Expression (C2) is put in the inversion integral to achieve the full time-dependent solution of  $u'_x$ . From (64) in Section 5 this can be written as

$$U = \left( \frac{q\Omega k_y}{k_\perp} \right) e^{i k_x(t)x} \int_{\tilde{\Gamma}} \hat{u}(x, \theta) e^{-i\tau\theta} d\theta, \quad (C5)$$

where  $\theta = x - x_c$  and  $\tilde{\Gamma}$  is a suitable contour in  $\theta$  space. Needless to say, general initial conditions do not yield closed forms for  $A$  and  $B$ , let alone  $U$ . However, some progress can be made if we take the asymptotic limit of large time  $\tau \gg 1$ . According to the Riemann-Lebesgue lemma the dominant contribution to the  $\theta$  integral occurs when  $\theta$  is small because of the  $\exp(-i\tau\theta)$  factor. Consequently, we expand  $A$ ,  $B$ ,  $u_+$ , and  $u_-$  in  $\theta$ . For  $A$  and  $B$  this means  $x_c \approx x$ , and so  $A = A(x)$  and  $B = B(x)$ . If  $\xi = y - x$  is a dummy variable, we get

$$A(x) \approx \frac{1}{W} \int_0^\infty \Lambda(x + \xi) \xi^{-1/2} [I_\nu(\xi) - I_{-\nu}(\xi)] d\xi. \quad (C6)$$

and a similar expression for  $B$ . We assume for the moment that these leading order expressions for  $A$  and  $B$  are nonzero and well-defined.

With  $A$  and  $B$  no longer depending on  $x_c$  (and hence  $\theta$ ), we can tackle the  $\theta$  integral just as in Booker and Bretherton (1967). For small  $\theta$  this integral is proportional to

$$\int_{\tilde{\Gamma}_e} \left( C(x) \theta^{1/2+\nu} + D(x) \theta^{1/2-\nu} \right) e^{-i\tau\theta} d\theta,$$

where  $\tilde{\Gamma}_e$  is that portion of the integration contour near  $\theta = 0$  and  $C(x)$  and  $D(x)$  are functions involving combinations of  $A$  and  $B$ . An order 1 variable is introduced,  $\zeta = i\tau\theta$  which establishes the basic time dependence of the integral. It can as a consequence be re-expressed as

$$\hat{C}(x) \tau^{-3/2+\nu} + \hat{D}(x) \tau^{-3/2-\nu},$$

where the new functions  $\hat{C}$  and  $\hat{D}$  involve integrals of the form

$$\int_0^\infty \zeta^{1/2\pm\nu} e^{-\zeta} d\zeta,$$

which may be integrated numerically.

Finally, we write down the long time fate of a localised initial condition. Given  $k_y$  and  $k_z$  we have

$$u'_x \propto e^{i k_x(t)x + i k_y y + i k_z z} t^{-3/2} \left( \hat{C}(x) t^\nu + \hat{D}(x) t^{-\nu} \right). \quad (C7)$$

The mode decays algebraically, with oscillatory behaviour when  $\nu$  is imaginary (i.e.  $\beta > 1/2$ ). The spatial structure of the solution is a shearing wave localised within an ‘envelope’ defined by the functions  $\hat{C}$  and  $\hat{D}$ , which in turn depend on the initial condition selected.

## C3 The behaviour of the $A$ and $B$ functions

To derive the main result we assumed that the leading order terms of  $A$  and  $B$  are nonzero and well behaved when  $\theta$  is small. In this subsection we attempt to justify these assumptions. In (C6) we expand  $\Lambda(x + \xi)$  in a Taylor series around  $x$  and truncate at some order  $N$ . This supplies a reasonable approximation as the dominant contribution to the integral comes from near  $\xi = 0$ ; moreover  $u_+$  decays rapidly with  $\xi$  (like  $e^{-\xi}$ ). The first term in the expansion is computed, and we find

$$A(x) \approx \frac{\sin(\pi\nu) \Gamma\left(\frac{1-2\nu}{4}\right) \Gamma\left(\frac{1+2\nu}{4}\right)}{\pi\sqrt{2}W} \Lambda(x) + \dots$$

A similar expression exists for  $B$ . Thus the leading order terms exist and are regular. We can thus be assured that generally  $A$  and  $B$  are both nonzero and well behaved.

## APPENDIX D: DISPERSION RELATION FOR INSTABILITY IN A THREE-DIMENSIONAL SLENDER TORUS

The full dimensionless dispersion relation which issues from the solvability of (67) at  $x = \pm s$  can be expressed as

$$\chi_4(\bar{\sigma}) \cdot \bar{\sigma}^4 + \chi_3(\bar{\sigma}) \cdot \bar{\sigma}^3 + \chi_2(\bar{\sigma}) \cdot \bar{\sigma}^2 + \chi_1(\bar{\sigma}) \cdot \bar{\sigma} + \chi_0(\bar{\sigma}) = 0, \quad (D1)$$

where

$$\begin{aligned} \chi_4 &= 4q^4 (S_{1+\nu}^{1-\nu} - S_{1-\nu}^{1+\nu}), \\ \chi_3 &= 2iq^3 \{ (q - 4 - 2\nu q)(S_{\nu}^{1-\nu} - S_{1-\nu}^{\nu}) \\ &\quad + (q - 4 + 2\nu q)(S_{1+\nu}^{-\nu} - S_{-\nu}^{1+\nu}) \}, \\ \chi_2 &= 8q^2(2 - q)(1 + \tilde{k})(S_{-\nu}^{\nu} - S_{\nu}^{-\nu}) \\ &\quad + 2sq^2(6 - 8q + q^2 + \tilde{k}(6 - 4q) - 2\nu q^2)(S_{\nu}^{1-\nu} + S_{1-\nu}^{\nu}) \\ &\quad - 2sq^2(6 - 8q + q^2 + \tilde{k}(6 - 4q) + 2\nu q^2)(S_{-\nu}^{1+\nu} + S_{1+\nu}^{-\nu}) \\ &\quad + 8q^4 s^2 (S_{1+\nu}^{1-\nu} - S_{1-\nu}^{1+\nu}), \\ \chi_1 &= -2iq^2 s \{ 4(2q - 3)(1 + \tilde{k})\nu(S_{-\nu}^{\nu} + S_{\nu}^{-\nu}) \\ &\quad + s(12 - 4q - q^2 - 4\tilde{k}(2q - 3) + 2\nu q^2)(S_{\nu}^{1-\nu} - S_{1-\nu}^{\nu}) \\ &\quad + s(12 - 4q - q^2 - 4\tilde{k}(2q - 3) - 2\nu q^2)(S_{-\nu}^{1+\nu} - S_{1+\nu}^{-\nu}) \}, \\ \chi_0 &= s^2 \{ 4[9 - 3q^2 + \tilde{k}(3 - 2q)^2](1 + \tilde{k})(S_{-\nu}^{\nu} - S_{\nu}^{-\nu}) \\ &\quad + 2q^2 s(-6 + q^2 + \tilde{k}(4q - 6) - 2\nu q^2)(S_{1-\nu}^{\nu} + S_{\nu}^{1-\nu}) \\ &\quad - 2q^2 s(-6 + q^2 + \tilde{k}(4q - 6) + 2\nu q^2)(S_{1+\nu}^{-\nu} + S_{-\nu}^{1+\nu}) \\ &\quad + 4q^4 s^2 (S_{1+\nu}^{1-\nu} - S_{1-\nu}^{1+\nu}) \}, \end{aligned}$$

in which  $\tilde{k} = (k_z/k_y)^2$  and where we have used the shorthand

$$S_{\nu}^{\mu} = I_{\mu}(i\bar{\sigma} + s) I_{\nu}(i\bar{\sigma} - s).$$

When  $\sigma \sim s \ll 1$ , Equation (D1) reduces to (68) after using the scaling

$$S_{\nu}^{\mu} \sim s^{\nu+\mu}.$$

Consequently, we find only the last three terms in (D1) contribute to the leading order balance.